

Julius-Maximilians-Universität Würzburg
Fakultät für Physik und Astronomie
Lehrstuhl für Astronomie



Bachelorarbeit

FACT - Observations at Large Zenith Distance

Autor: Bernd Schleicher

Betreuer: Prof. Dr. K. Mannheim

Abgabedatum: 31.03.2017

Zusammenfassung

Als Aktive Galaxienkerne (AGN) bezeichnet man Zentralregionen von Galaxien, die mehr Strahlung aussenden als der Rest der Galaxie. Sie emittieren Strahlung entlang des gesamten elektromagnetischen Spektrums und weisen zwei Maxima in der spektralen Energieverteilung auf. Eine Unterart von AGN sind Blazare, welche Strahlung im TeV Energiebereich aussenden. Diese Art von Quellen zeichnen sich außerdem durch extreme Variabilität auf Zeitskalen von Minuten bis zu Jahren aus, und die zugrundeliegenden physikalischen Prozesse für die Entstehung der Strahlung sind noch nicht vollständig verstanden. Im Wesentlichen gibt es zwei Modelle für die Entstehung der Strahlung, die leptonischen und die hadronischen Modelle. Deshalb ist es wichtig diese Quellen über längere Zeiträume zu beobachten, um die verschiedenen Theorien zu testen. Für Beobachtungen von Gammastrahlung mit TeV-Energien werden Teleskope verwendet, die das Cherenkov-Licht, das beim Eintritt der Gamma-Teilchen in die Erdatmosphäre entsteht, beobachten. Das abbildende Luft-Cherenkov Teleskop FACT benutzt auf Halbleiter basierende Photodetektoren, da diese nicht beschädigt werden, wenn sie zu viel Hintergrundlicht ausgesetzt werden. Dies ermöglicht längere Beobachtungszeiten und sogar Beobachtungen während Vollmond. Das First G-APD Cherenkov Telescope (FACT) ist das erste Teleskop, das diese Art von Detektoren verwendet. Um eine Quelle so viel wie möglich zu beobachten, ist es nötig, auch unter nicht idealen Bedingungen, wie zum Beispiel große Zenitwinkel, Messungen durchzuführen. Solche Daten können mit der Standard FACT Analyse nicht optimal ausgewertet werden, da diese für kleine Zenitwinkel optimiert wurde. Aus diesem Grund wird in dieser Arbeit die Untergrundunterdrückung der Standard FACT Analyse für Messungen bei allen Zenitwinkeln angepasst. Dazu muss der Effekt des Zenitwinkels auf die Analyse verstanden werden. Es wurden Daten von Beobachtungen des Krebsnebels bei gutem Wetter verwendet um die Untergrundunterdrückung auch bei großen Zenitwinkeln anzupassen. Der Krebsnebel wird in der TeV-Astronomie als konstante Quelle angesehen und dient deshalb zur Kalibrierung. Für die Untergrundunterdrückung werden die zuvor bestimmten Bildparameter eines gemessenen Ereignisses verwendet. Mit einem Datensatz von Krebsdaten, mit Messungen bis zu 60° Zenitwinkel, der in 5° Schritten über den Zenitwinkel aufgeteilt ist, wurde untersucht wie sich diese Bildparameter mit dem Winkel verändern. Hierzu wurden Histogramme der einzelnen Parameter erstellt und die Veränderung des Mittelwertes über den Winkel analysiert und die Schnitte, die in der Untergrundunterdrückung verwendet werden, angepasst. Mit diesen neuen Schnitten wurde die Lichtkurve des Krebsnebels erzeugt und mit der verglichen, die mit der Standard FACT Analyse erstellt wurde. Dabei konnte ein leichter Rückgang der Exzessrate und der dazugehörigen Fehler festgestellt werden. Ebenfalls wurde dieser Vergleich der Lichtkurven für Messungen des BL Lacertae-Objektes 1ES 1959+650 gemacht. Da diese Quelle allerdings erst bei ungefähr 35° Zenitwinkel auf La Palma kulminiert, ist es wichtig die Analysemethoden für diese großen Zenitwinkel zu optimieren. 1ES 1959+650 ist eine sehr variable Quelle die in den Anfangsjahren von FACT kaum Aktivität gezeigt hat, allerdings seit dem Jahr 2015 sehr aktiv ist. Im Jahr 2016 zeigte sich zwei Helligkeitsausbrüche mit einer Exzessrate von mehr als $50 \frac{\text{events}}{\text{h}}$. Für 1ES 1959+650 wurden im Jahr 2016 fünf ATELS verfasst, da diese Quelle so einen variablen und hohen Fluss gezeigt hat. Durch Beobachtungen von anderen Teleskopen können dann möglichst viele Daten von den Helligkeitsausbrüchen erhalten werden und auch den Abfall der Lichtkurve so genau wie möglich bestimmt werden. Die gemessenen Daten können für Multi-Wellenlängen Kampagnen und für Multi-Messenger Astronomie verwendet werden.

Abstract

Active Galactic Nuclei (AGN) are central regions of galaxies outshining the rest of the host galaxy. AGN emit radiation across the electromagnetic spectrum showing two distinct peaks in the spectral energy distribution. A subtype of AGN are blazars, which are sources for radiation in TeV energies. This type of source exhibit extreme variability on timescales from minutes to years, and the underlying physical processes of the emitted radiation are not completely understood yet. Mainly there are two types of models, the lepton and the proton models. In order to test the theoretical models of blazars, it is necessary to observe such sources as much as possible. Observations in the TeV regime are made by observing Cherenkov light, which arises when the gamma particles enter the Earth atmosphere. To maximize the observation time, the Imaging Air Cherenkov Telescope FACT is using silicon based photosensors (SiPM), because they do not degrade when exposed to bright light providing the possibility to observe during full moon. The First G-APD Cherenkov Telescope (FACT) is the first telescope that uses such detectors. By increasing the observation time it is not possible to only have the best conditions. As the atmosphere is part of the detector, the amount of measured light decreases with increasing zenith distance, complicating the analysis for these conditions. The standard FACT analysis is optimized for observations with small zenith distance. In this work, the background suppression of the FACT analysis chain is adapted to large zenith distance. Data from the Crab Nebula are used for this, because the Crab Nebula is a stable source that is used in TeV-astronomy as a standard candle. To remove the background events the image parameters of an event are used. Data of the Crab Nebula up to zenith distance of 60 degree, binned in 5 degree steps, are used to investigate the change of these image parameters. The changes in the mean value of each parameter over the zenith distance are analysed. Based on this, the changes are used to determine zenith distance dependent background cuts. Using these new cuts, a light curve of Crab data is plotted and compared with a light curve resulting of the standard FACT analysis. The changes are a decrease in the excess rate and the corresponding errors. Such a comparison of the light curve is also made for the BL Lac object 1ES 1959+650. A zenith distance dependent analysis is very important for this source, because it culminates for La Palma at about 35 degree. This source was inactive in the first years of FACT observations, but since 2015 1ES 1959+650 is an active and very variable source. In 2016, this target showed two flaring nights with excess rates over $50 \frac{\text{events}}{\text{h}}$. FACT sent five ATELS during 2016 on this source, because it showed a high and variable flux. By combining FACT data with data from other telescopes, the flaring nights and the decrease of the light curve can be studied. The data can be used in multi-wavelength and multi-messenger astronomy studies.

Inhaltsverzeichnis

1	Introduction	9
1.1	Active Galactic Nuclei	9
1.1.1	Historical Classification	9
1.1.2	Unified Theory of AGN	10
1.1.3	Blazars	10
1.2	The FACT Project	10
1.2.1	Geiger-Mode Avalanche Photodiodes	11
1.2.2	Robotic Operation	11
1.2.3	Long-term Monitoring of Bright TeV Blazars	13
2	Datataking and Analysis	15
2.1	Imaging Air Cherenkov Technique	15
2.2	Analysis	16
2.2.1	Calibration	16
2.2.2	Image Cleaning	16
2.2.3	Image Parameter Calculation	17
2.2.4	Background Suppression	18
2.2.5	Signal Reconstruction	18
3	Zenith Depending Cuts for the Background Suppression	21
3.1	Datasample	21
3.2	Image Parameter Distributions	21
3.2.1	<i>SlopeSpreadWeighted</i>	21
3.2.2	<i>Area</i>	21
3.2.3	<i>Size</i>	24
3.2.4	<i>Conc_{core}</i>	24
3.2.5	<i>Conc_{COG}</i>	24
4	Results	29
4.1	Crab Nebula	29
4.2	1ES 1959+650	29
5	Summary and Outlook	37
5.1	Zenith Dependent Cuts	37
5.2	Flaring Activity of 1ES 1959+650	37
6	Acknowledgement	43

1 Introduction

Active Galactic Nuclei (AGN) are the brightest objects in the sky and show radiation ranging from radio to gamma rays. The centre of AGN consist of a supermassive black hole, which effectively produces energy by accreting matter from the surrounding accretion disk. Those extra galactic objects are observed in the whole electromagnetic spectrum, and they are subject of ongoing research. Most of the observations have unobserved time gaps because of used methods. It is known that the emission of AGN is variable, so multi-wavelength campaigns over the whole spectrum are needed to investigate the underlying processes. For this, long-term monitoring with small as possible time gaps are needed. In order to increase the observation time during bright conditions, FACT (First G-APD Cherenkov Telescope) is equipped with silicon based photomultiplier tubes (SiPM), which is the first one using this kind of detectors for the Imaging Air Cherenkov Technique. This enables the possibility to observe also during full Moon nights. [11] FACT is built as a low cost telescope for proofing the principle usage of SiPM in Cherenkov astronomy and for long-term monitoring of bright TeV-sources.

At present, the FACT analysis chain is optimized for observations with a zenith distance smaller than 30 deg. To enlarge the observation time, it is also necessary to go to larger zenith distance. To study sources, like the blazar 1ES 1959+650, which culminate at zenith distance of about 35 deg, the analysis needs to be optimized also for those conditions.

In this work, a zenith distance dependent background suppression for the analysis is determined. This is done by using data from the Crab Nebula, which is used as a standard candle in Cherenkov astronomy. Furthermore a light curve of Crab data is generated with the changed background suppression to illustrate the effect of changes. Also the light curve of 1ES 1959+650 is determined.

At first, an introduction to AGN, especially blazars, and the FACT project is given. In Chapter 2, the Imaging Air Cherenkov technique and the FACT analysis chain are described. Section 3 shows the derivation of the zenith distance dependent background suppression cuts based on a Crab Nebula dataset. Finally, the impact of the new suppression is shown in section 4, by providing light curves of the Crab Nebula and the blazar 1ES 1959+650 for data from the years 2013 till 2016.

1.1 Active Galactic Nuclei

1.1.1 Historical Classification

The main targets of FACT observations apart from the Crab Nebula are Active Galactic Nuclei (AGN). Historically, they were classified by their properties. They can be divide in the three classes Type 0 (unusual), Type 1 (Broad Line) and Type 2 (Narrow Line). And this classes can be split again in radio loud and radio quite galaxies: [16] [26]

- Type 1 AGN have a strong continuum spectra from infra-red to x-ray and broad line emission. The radio quite ones are Seyfert 1 galaxies and radio quiet Quasi-Stellar Objects (quasar). Radio quiet quasars have a higher luminosity than Seyfert 1 galaxies. Examples for the radio loud galaxies are Broad-Line Radio Galaxies (BLRG) and radio-loud quasars, which can be Steep Radio Quasars (SSRQ) or Flat Spectrum Radio Quasars (FSRQ) depending on their radio spectra shape.
- Type 2 AGN have narrow emission lines and show only faint or no continuum emission. Seyfert 2 galaxies are radio quiet narrow line AGN. Radio quiet Type 2 AGN are named

Narrow-Line Radio Galaxies (NLRG). There are two kinds of them, the Fanaroff-Riley type 1 radio galaxies and the brighter Fanaroff-Riley type 2 radio galaxies [9].

- Type 0 AGN show unusual spectral characteristics. About 10 % of the radio-quiet AGN called Broad Absorption Line quasars (BAL quasars), because they have special broad P-Cygni-like absorption lines in optical and ultraviolet wavelengths. [25] This BAL quasars are candidates for Type 0 AGN. Radio loud unusual AGN are for example the BL Lacertae (BL LAC) objects, with some missing emission or absorption lines. Some Type 1 AGN quasars have similar continuum emission to BL LAC objects. They called Optically Violently Variable (OVV) quasars, Highly Polarized Quasars (HPQ) Core-Dominated Quasars (CDQ) or FSRQ. Summarized the radio loud Type 0 AGN called Blazars and show very rapid variability, high and variable polarization, high brightness temperatures and superluminal velocities of compact radio cores.

1.1.2 Unified Theory of AGN

The common opinion is the unified theory of AGN, which suggests that all these AGN classes are the same kind of galaxies and the different properties can be described mainly as a function of the viewing angle to the AGN. Such an AGN is composed of a black hole in the middle surrounded by a hot accretion disk, which itself is encircled by a large dust torus. Perpendicular to the plane of the accretion disk and dust torus, there are two jets streaming out of the centre of the AGN. These jets are the outflow of relativistic particles. [28]

1.1.3 Blazars

The most prominent sources for radiation in the Very High Energy region are blazars. The line of sight is pointing at or very close to the relativistic jet. Blazars are highly variable on time scales from years to minutes and their Spectral Energy Distribution (SED) shows two peaks. The underlying emission process of the lower energy peak is synchrotron radiation from accelerated electrons in the jet.[3] For the higher energy peak are some models discussed. There are mainly two types of models, the lepton and proton models. Leptonic models describe the second peak as a peak made of inverse Compton Scattering. They can be distinguished in two models. If the electron itself produces the photon by synchrotron radiation it is called Synchrotron-Self-Compton (SSC) model or if the origin of the photon is from the surrounding gas clouds it is called External Radiation Compton (ERC) model. [24] The proton models suppose that the electrons, that are responsible for the synchrotron peak, are secondary particles of accelerated protons that interact with soft photons by photo-production of pions. The neutral pions decay in photons, which create through pair production the electrons for synchrotron peak. An electromagnetic cascade can be started, which produces photons with energies to the TeV range and below.[18] To investigate which model of the VHE emission fits better, the SEDs and their temporal progress is used.

1.2 The FACT Project

There are two possible ways to observe gamma rays from Active Galactic Nuclei (AGN). The direct method is observing gamma rays with satellites from space. But for very-high-energy (VHE) observations large detector volumes would be needed, what is really expensive. For the VHE radiation, the better way to observe is with an indirect method called the Imaging Air Cherenkov Technique. This method uses the atmosphere as a part of the detector. The gamma



FIG. 1: First G-APD Cherenkov Telescope during observations. Credit: Daniela Dorner

rays induce particle-showers in the atmosphere, and if the secondary particles travel faster than the speed of light in the medium, they produce Cherenkov light. This Cherenkov light can be observed from ground based telescopes. This so called Imaging Air Cherenkov Telescopes use a mirror to focus the picture of the shower to a camera. The First G-APD Cherenkov Telescope (FACT) is such a telescope and operates since October 2011. It is located at the Observatorio del Roque de los Muchachos on the Canary Island of La Palma at a height of 2200 meter above sealevel. The Telescope uses the refurbished HEGRA CT3 mount and the mirror of HEGRA CT1 with a mirror area of 9.5 m^2 . Figure 1 shows the telescope during observations with bright moon conditions. The major goals of the FACT project are the long-term monitoring of bright TeV blazars, the proof of the use of Geiger-mode Avalanche Photodiodes (G-APD) in Cherenkov Astronomy and the robotic operation of the telescope. [8]

1.2.1 Geiger-Mode Avalanche Photodiodes

FACT is the first Imaging Air Cherenkov Telescope that operates a camera with Geiger-mode Avalanche Photodiodes (G-APD) instead of photomultiplier tubes (PMT). These silicon based photomultiplier have shown that they provide stable performance over a long time. [7] Because of a stable and homogeneous gain no external calibration is needed. Another big advantage of G-APDs is that they can be used during bright conditions without degrading. Even if FACT points straight to the full moon events can be detected. In Figure 2(a) is the FACT camera pointing directly to the full moon shown and by disabling the power of the inner pixels it is possible to observe events (fig. 2(b)). [11] This allows more observation time during bright conditions, which is needed for minimizing the gaps for long term monitoring.

1.2.2 Robotic Operation

Currently, FACT is remotely controlled. In Figure 3, you see the web interface smartfact, which is used to control the telescope and monitor the system during observations. This interface is

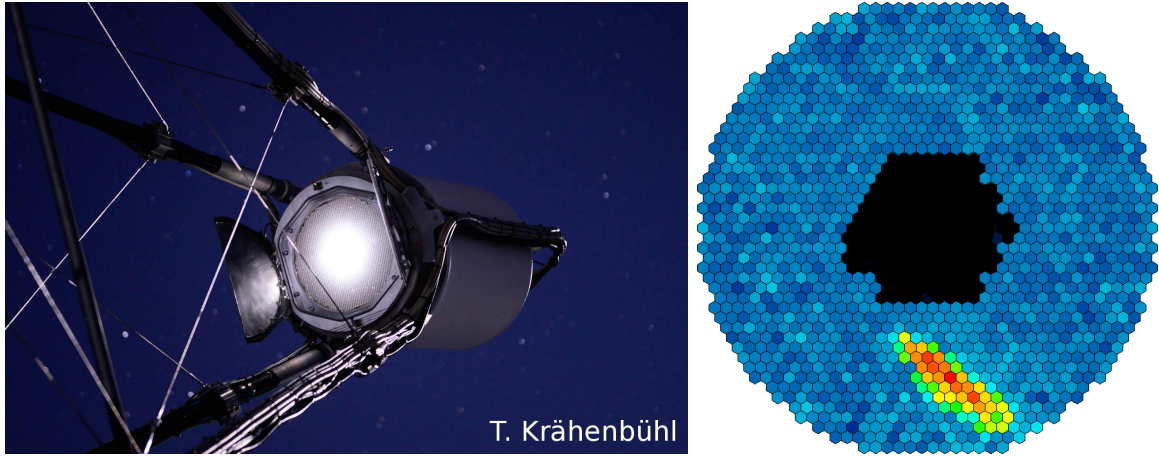


FIG. 2: FACT pointing to the full moon on 23.6.2013 [11]

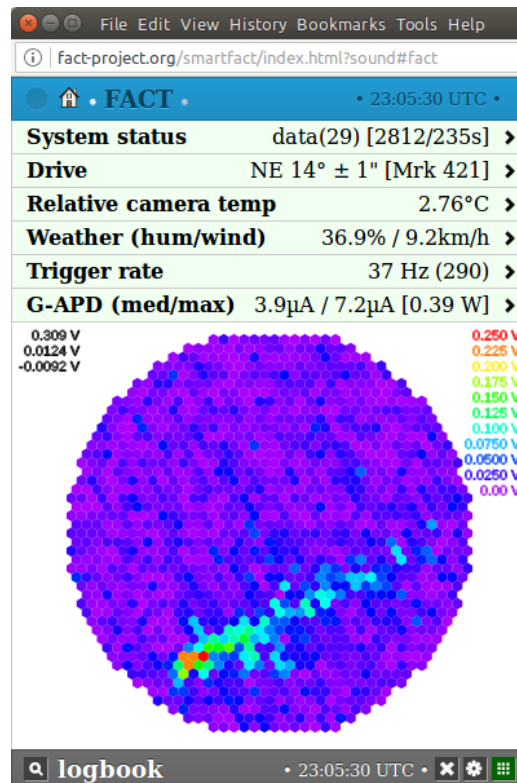


FIG. 3: Screenshot of the smartfact-interface. The telescope can be controlled with this interface. (<http://fact-project.org/smartfact>)

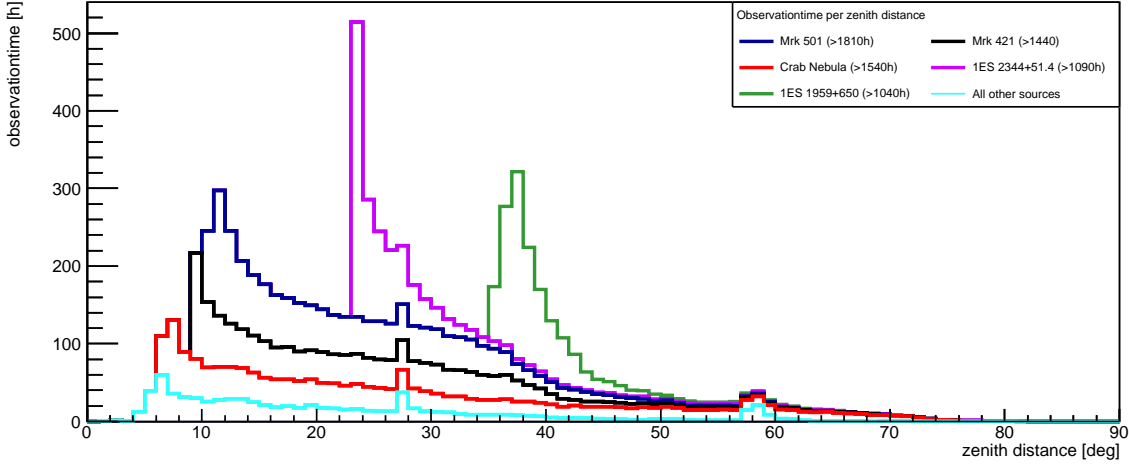


FIG. 4: Stacked histogram of the observed sources of FACT until November 2016 over the zenith distance. The peak at about 27 deg in the other sources histogram is caused by the culmination of PKS 0736+01 and at about 60 deg culminates PKS 2155-304.

optimized for low data traffic to give the shifter the opportunity to use it on his mobile phone. The system is automatized so that the shifter only has to start a script at the beginning of the night and to stop it in the morning. During the night, the shifter monitors the running system on smartfact.[8] For the future, it is planned to operate the Telescope with a shifter on call. A program named shifthelper monitors the running system during the night and calls the shifter if there is a problem which the system cannot solve on its own. At the moment the shifthelper is tested during the normal operation. For reasons of safety the startup and shutdown at the beginning and end of the night must be done by a human to ensure that there is nobody in the locked area around the telescope when starting data taking and to guarantee that the telescope is parked in the right direction in the morning. Another important point to do before changing the system to robotic operation is to implement a automated night summary which gives relevant informations about the nightly weather conditions and problems during the observation. Automatic operation increases the data taking efficiency and maximizes the observation time.

1.2.3 Long-term Monitoring of Bright TeV Blazars

Long-term monitoring of bright TeV blazars is necessary because the light curves are highly variable on timescales ranging from minutes to years. Long-term monitoring is also important for Multi Wavelength (MWL) campaigns, where the measurements of other wavelengths are combined with TeV data. This combined data allow research of the fundamental acceleration processes and related physics of the relativistic jets. The source sample of FACT is shown in Figure 4 as a function of the observed zenith distance.[20] The monitored sources are the blazars Mrk 412, Mrk 501, 1ES 1959+650 and 1ES 2344+51.4, which have been observed for more than 1000 h each. Also the Crab Nebula, a supernova remnant and used as a standard candle in VHE astronomy, is monitored. In the year 2016, FACT has taken more than 2300 h of physics data, because of the high data taking efficiency and minimized gaps.

2 Datataking and Analysis

2.1 Imaging Air Cherenkov Technique

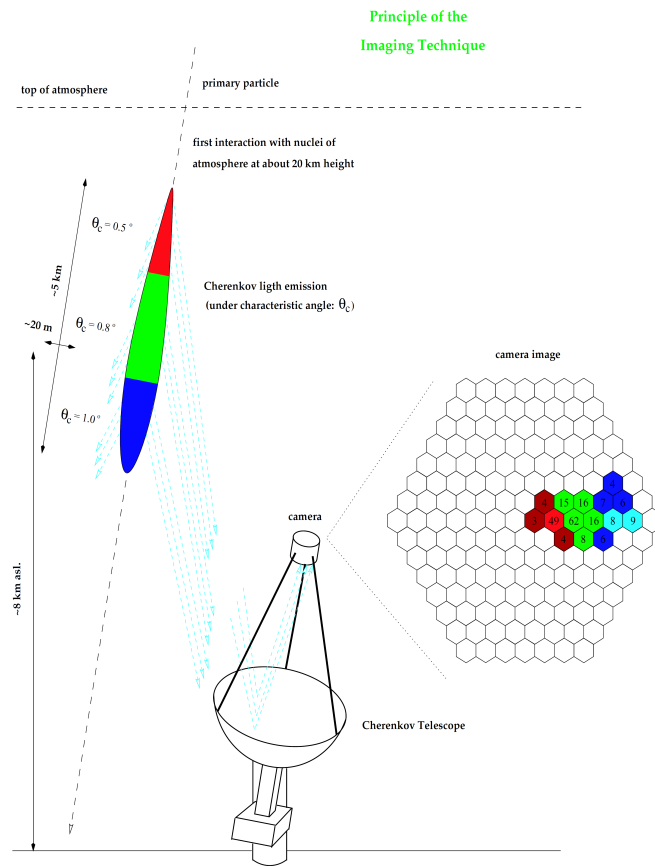


FIG. 5: Principle of the Imaging Air Cherenkov Technique. The incoming primary particle interacts with a nuclei of the atmosphere and produces a particle shower which emits Cherenkov light. This light is reflected by the mirror of the telescope and observed with a camera. [21]

If a high energetic particle hits the Earth's atmosphere, it interacts after a characteristic mean free path with particles of the atmosphere. This interaction generates secondary particles which have in the first order the same direction as the primary particle. These secondary particles interact as well with the surrounding particles and produce a particle shower. The speed of the particles in the shower can be almost the speed of light. If the speed of the particles is larger than the speed of light of the atmosphere it will emit Cherenkov light. There are two possible kinds of showers depending on the particle. Electromagnetic showers are produced by gamma particles and hadronic showers by hadrons mostly by protons. The leading processes in electromagnetic showers are pair production and bremsstrahlung. A hadronic shower however is dominated by strong and weak interactions and can have several subshowers. Because of this difference hadronic showers are much wider than an electromagnetic one. The different morphology of the showers is used to distinguish between gamma-like events and background. [5] Imaging Air Cherenkov Telescopes like FACT reflect the photons of emitted Cherenkov light with a mirror onto a camera to observe this emitted Cherenkov light from the particle showers. The principle of such a telescope is shown in fig. 5. In fig. 6, the images recorded by the FACT

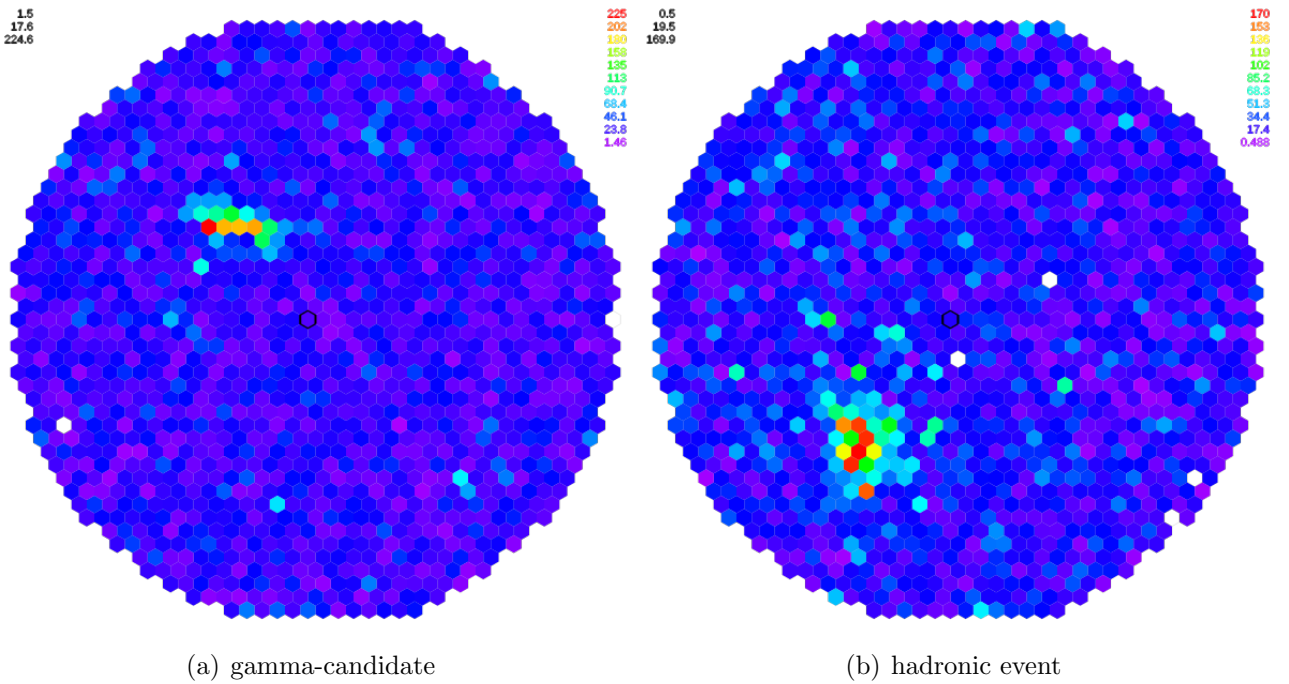


FIG. 6: Events seen through the FACT camera. The colour code shows the number of measured photons. This pictures are take from the eventviewer on the FACT homepage (<https://www.fact-project.org/viewer/>)

camera for a gamma-candidate (6(a)) and for a hadronic event (6(b)) are shown. The gamma-like event has a smooth ellipse like shape while the hadronic event has more small islands due to the subshowers.

2.2 Analysis

The Modular Analysis and Reconstruction Software (Mars)[6], that is based on ROOT, is used for the data analysis of FACT data. There are five steps of the analysis:[8]

2.2.1 Calibration

The first step is to extract the signal and interpolate bad pixels. For data taken before March 2014, the extracted signal was calibrated with an external light pulsar. The calibration with an external light pulsar is not needed any more because, the final version of the feedback system provides a stable and homogeneous gain. [4]

2.2.2 Image Cleaning

Using extracted signal and timing information all pixels not belonging to the shower image are removed. Pixels are only kept when the arrival time difference to neighbouring pixels is less than 17.5ns and the threshold is higher than 5.2 and for the neighbouring pixels higher than 3.3.

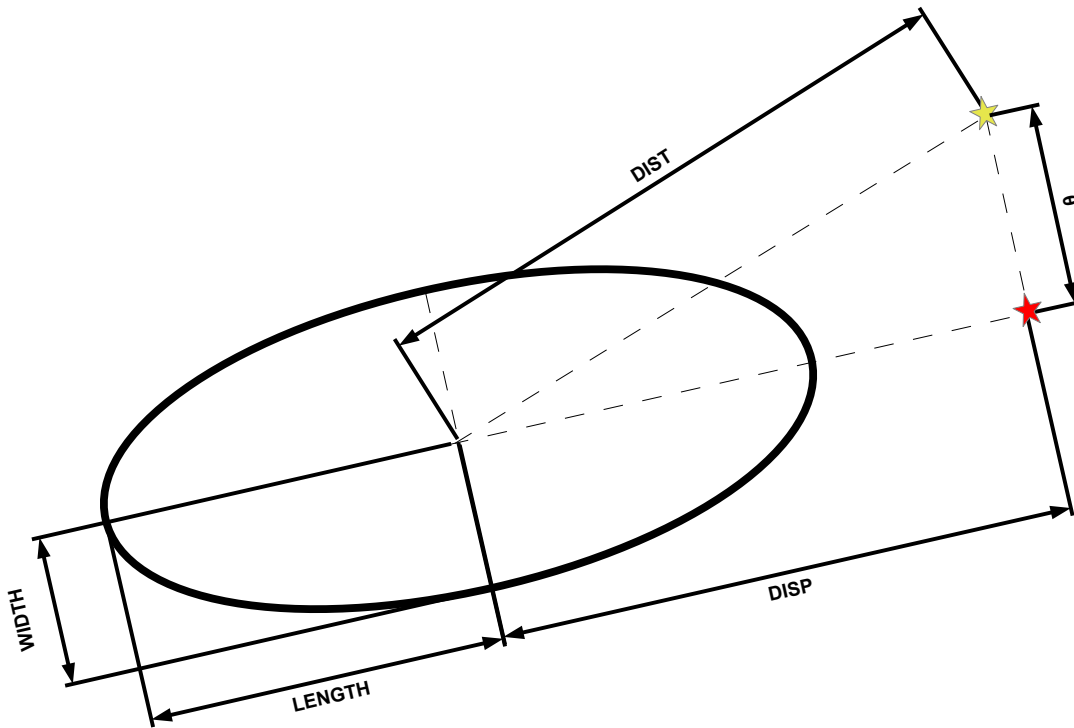


FIG. 7: Definition of the geometrical image parameters seen in the camera. The red star represents the reconstructed source and the yellow star the assumed source position.

2.2.3 Image Parameter Calculation

From the cleaned images several image parameters are calculated. These parameters are used to reconstruct the type of the shower and the origin and energy of the primary particle. Some of the important image parameters are:

- **Size:** total sum of photons belonging to the cleaned image
- **Length:** Length of the major axis of the reconstructed ellipse
- **Width:** Length of the minor axis of the ellipse
- **Dist:** Distance from the source to the center of the ellipse
- **Disp:** Distance from the center of the ellipse to the reconstructed source position
- **Theta (Θ):** Angular Distance between the reconstructed source position and the assumed position of the source
- **Area:** Geometrical Area of the ellipse $Length \cdot Width \cdot \pi$
- **NumUsedPixels** Number of pixel that survived the image cleaning
- **NumIslands** Number of Islands
- **Leakage1:** Ratio of the pixels used in the outer ring to the number of pixels in the shower

- **Leakage2:** Ratio of the pixels used in the two outer rings to the number of pixels in the shower
- **SlopeSpreadWeighted:** Spread of the evolution of the arrival time along the shower axis weighted with the size
- **Conc_{core}:** Ratio of the Size of the core pixel to the total Size
- **Conc_{COG}:** Ratio of the Size of the three pixel next to the center of gravity to the total Size
- **ZD** Zenith distance of the observed source

The geometrical image parameters are also shown in Figure 7.

2.2.4 Background Suppression

First, quality cuts are applied, which remove all events that cannot be reconstructed. The criteria therefore are:

- $NumIslands > 3.5$ or
- $NumUsedPixels < 5.5$ or
- $Leakage1 > 0.1$

Then the background suppression is done. Following cuts are used at the moment:

- $0.18 < SlopeSpreadWeighted < 0.68$
- $\log_{10}(Area) < (\log_{10}(Size) - 2) \cdot 1.1 - 1.55$
- $Conc_{core} > 0.13$
- $Conc_{COG} > 0.15$

As a last step of the Background suppression the parameter $Disp = \xi \cdot (1 - Width/Length)$ is calculated according to [17], where the correction term ξ is:

$$\xi = 1.14136 + 0.0681437 \cdot Slope + 2.62932 \cdot \log_{10}(Leakage1 + 1) + \begin{cases} 0.0507821 \cdot (\log_{10}(Size) - 1.51279)^2, & \log_{10}(Size) > 1.51279 \\ 0, & \log_{10}(Size) < 1.51279 \end{cases}$$

2.2.5 Signal Reconstruction

In the next step, the parameter Θ^2 is calculated. It is the angular distance between $Dist$ and $Disp$. By plotting a histogram of Θ^2 , it is decided, if the event origin is the source. Such a Thetasquaredplot of a flaring night on 14.04.2013 of Mrk 421 is shown in Figure 8. The black crosses are the on-measurements and the gray area are the off-measurements. On the left side, of the dashed line the signal region is shown, and the excess events are calculated by subtracting the off-measurements from the on-measurements of the signal region. To get the excess rate, the excess events are divided by the ontime of the measurement. The next step is to reconstruct the energy of each event by the use of monte carlo simulations, in order to calculate the flux. Due to the fact that simulations need a lot of computing time and that a lot of simulated events needed to reconstruct the energy, the excess rate light curves are used for example to give alerts of flaring sources to other instruments.

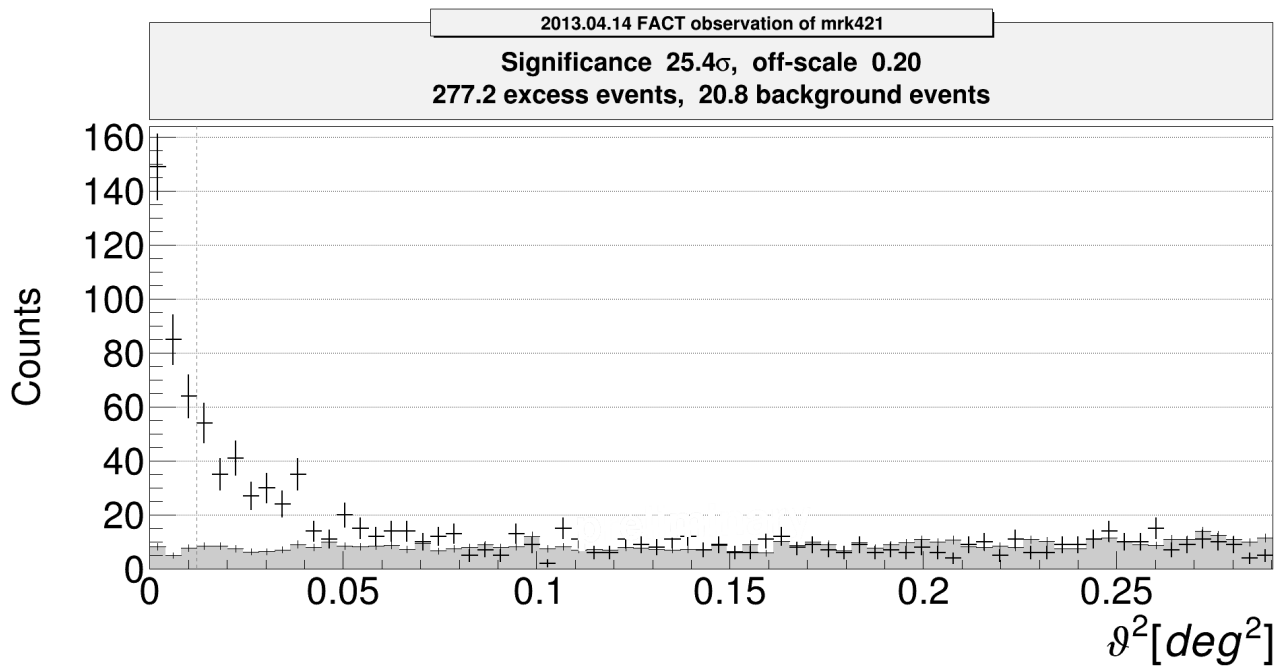


FIG. 8: Thetasquaredplot from observations of Mrk 421 during the flaring night on 14.04.2013. The black crosses are the events of the on-region, while the gray area are the events of the five off-regions scaled with a factor of 0.2. The ontime of this measurement is 2.7 h.

3 Zenith Depending Cuts for the Background Suppression

The Imaging Air Cherenkov Technique uses the atmosphere as a part of the detector. One big advantage of this is a large detector volume. But the different conditions influence the detection of the events. There are several influences like the ambient light, the geomagnetic field, the atmospheric profile and the zenith distance of the observed object. For the long-term monitoring, it is important to enlarge the visibility window and because of that is crucial to observe sources at large zenith distance and to optimize the analysis for observations at this conditions. So a zenith distance dependent background suppression is needed to increase the excess rate of the taken data.

3.1 Datasample

The Crab Nebula is a supernova remnant, from a supernova that took place in the year 1054 [19] and it is the first gamma-ray source found by an Imaging Air Cherenkov Telescope, the Whipple Observatory 10 m reflector. [27] The gamma-ray spectrum with an energy E above 100 GeV of the Crab Nebula is dominated from inverse Compton scattering of synchrotron photons of the relativistic electrons. It is found that in this energy region the spectrum of the Crab Nebula is mostly stable [2]. Crab is a standard-candle at TeV energies and perfect to study the effect of large zenith distance observations on the background suppression. A datasample of Crab data with more than 750 hours of observation time is used. The trigger threshold of all used data is smaller than 450 photons. For every day of the datasample, a manual datacheck is made by using the informations that are available in the logbook, to exclude days with bad weather conditions, technical problems and also days where the MAGIC Lidar shoots in the Field of View of FACT during observations of Crab. The MAGIC Lidar is a system to measure the atmospheric transmission within the field of view of MAGIC. It uses a laser beam to observe the transmission for different heights.[12] The datasample is binned in zenith distance, for values between 5 deg and 60 deg with a bin width of 5 deg.

3.2 Image Parameter Distributions

To understand how the image parameters change for observations with different zenith distance, one can look at the distribution of the single image parameters for different zenith distances. For this, the summary output of the macro ganymed.C is used. It includes all events that survived the image cleaning, which means its mostly hadronic background.

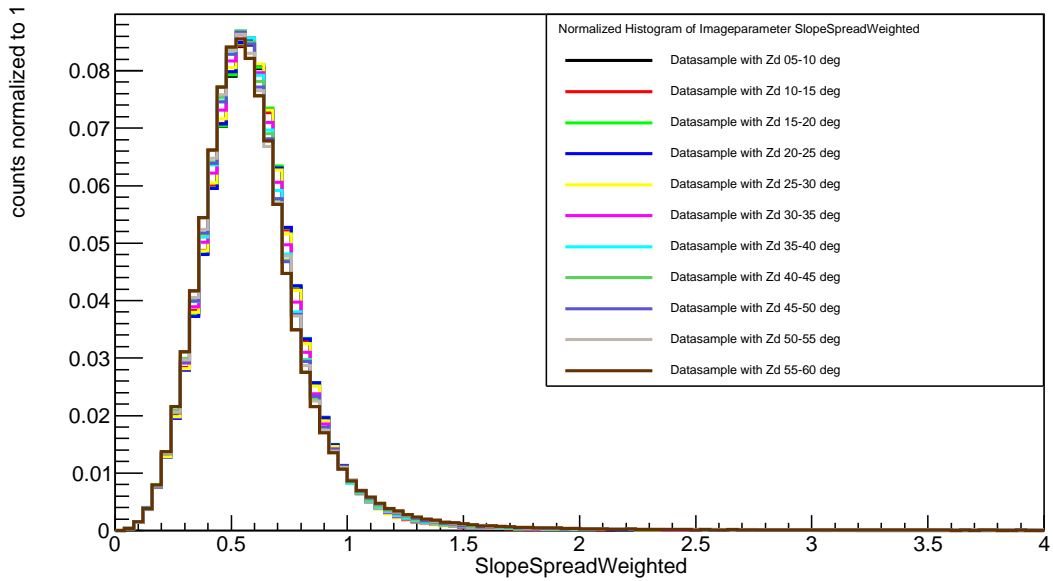
3.2.1 *SlopeSpreadWeighted*

Figure 9(a) shows the distribution of the parameter *SlopeSpreadWeighted* for the datasamples with the different zenith distance ranges. To compare the different ranges all distributions are normalized to one. As we can see this image parameter changes not significantly, with a change of the zenith distance. The mean value of the image parameter *SlopeSpreadWeighted* is shown in Figure 9(b) and also shows no clear change in zenith distance. So there is no need of a zenith distance correction for this background cut.

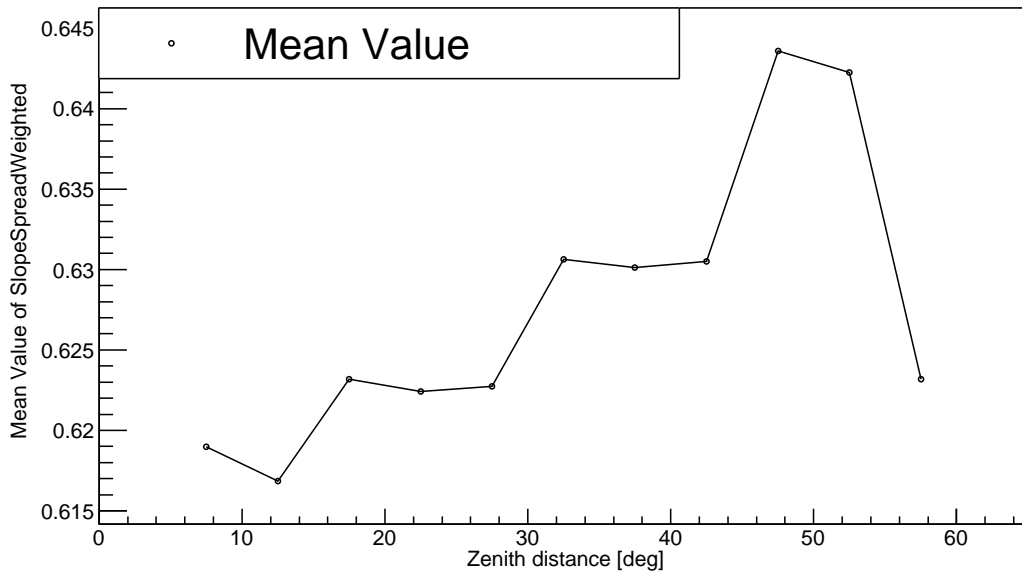
3.2.2 *Area*

The zenith distance dependency of the image parameter *Area* is as well investigated by plotting its normalized distribution for different zenith distance samples. The result is shown in Figure

3 Zenith Depending Cuts for the Background Suppression

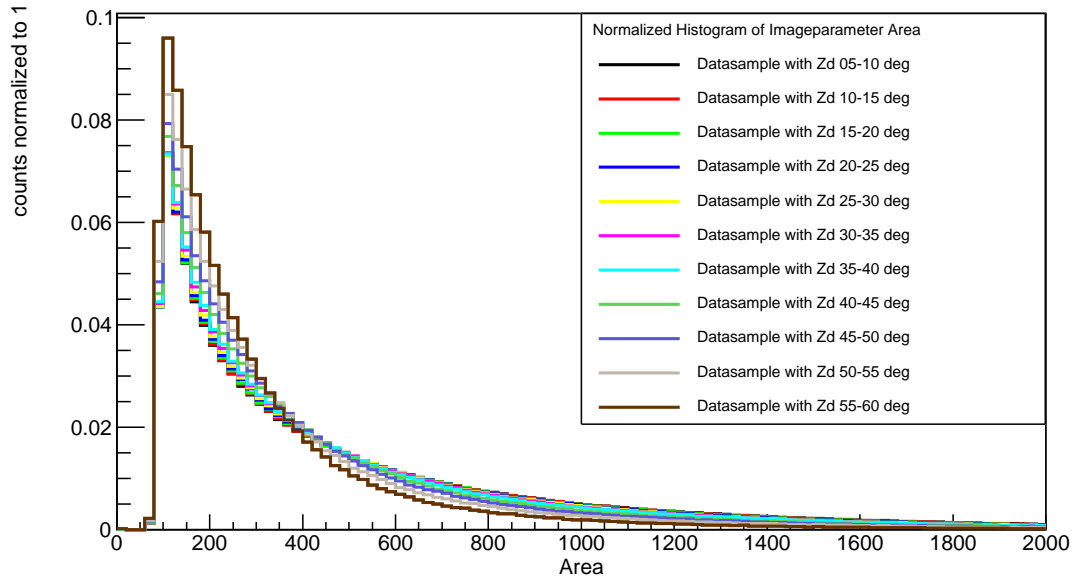


(a)

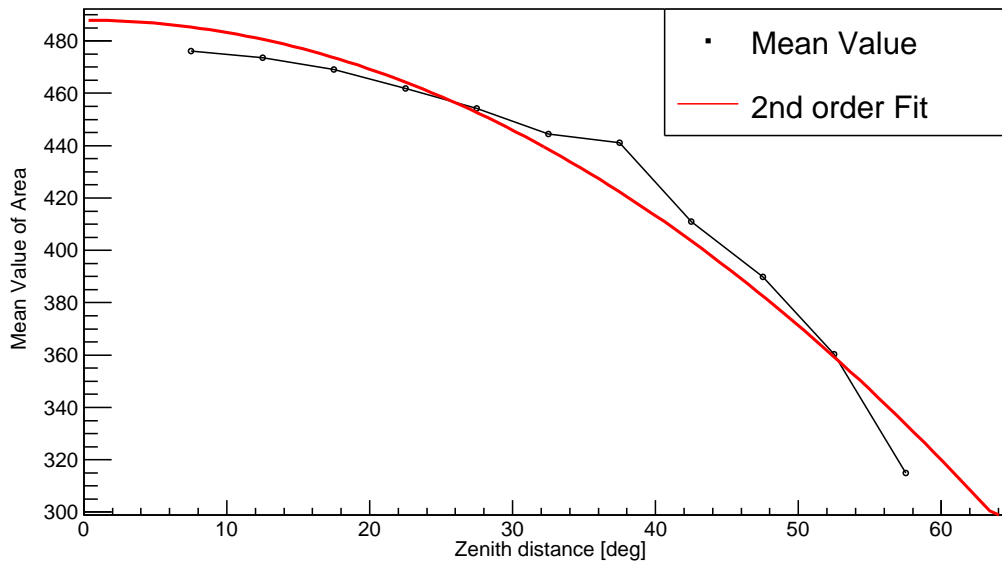


(b)

FIG. 9: Distribution of the image parameter *SlopeSpreadWeighted* normalized to one for the different zenith distance ranges on the upper plot. The lower plot shows the mean value of the distribution as a function of the zenith distance.



(a)



(b)

FIG. 10: Distribution of the image parameter *Area* normalized to one for the different zenith distance ranges (upper plot). The lower plot shows the mean value of the distribution as a function of the zenith distance

3 Zenith Depending Cuts for the Background Suppression

10(a). One can see that for larger zenith distance the distribution drops down faster than for lower zenith distance. Due to this faster drop down, the mean value that is shown in Figure 10(b) decreases as a function of the zenith distance. To correct the cut for this decrease, the mean value is fitted with a parabolic fit ($\overline{Area} = \alpha + \beta \cdot (ZD)^2$). The result for the fitting parameters are:

$$\alpha = 487.902 \pm 5.08946$$

$$\beta = -0.046658 \pm 0.00303542$$

Applying this result to the background suppression cut, the new cut looks like:

$$\log_{10}(Area + 4.6658 \cdot 10^{-2} \cdot (ZD)^2) < (\log_{10}(Size) - 2) \cdot 1.1 - 1.55$$

3.2.3 Size

The image parameter *Size* is analysed in the same way that *SlopeSpreadWeighted* and *Area*. In Figure 11, the result is shown. The plot 11(b) is zoomed version of the normalized distribution (11(a)). The mean value of this distribution also changes drops for larger zenith distance. The mean value is also fitted with a parabolic fit ($\overline{Size} = \alpha + \beta \cdot (ZD)^2$). The result is:

$$\alpha = 203.228 \pm 1.31691$$

$$\beta = -0.0154657 \pm 0.00078542$$

Now the background cut for the image parameters *Size* and *Area* is corrected to:

$$\log_{10}(Area + 4.6658 \cdot 10^{-2} \cdot (ZD)^2) < (\log_{10}(Size + 1.54657 \cdot 10^{-2} \cdot (ZD)^2) - 2) \cdot 1.1 - 1.55$$

3.2.4 Conc_{core}

Figure 12 shows the normalized distribution of the image parameter *Conc_{core}* and how the mean value changes with the zenith distance. There is no significant change in the distributions and the mean values, so that there is no dependency of this image parameter to the zenith distance and therefore the cut will not be changed.

3.2.5 Conc_{COG}

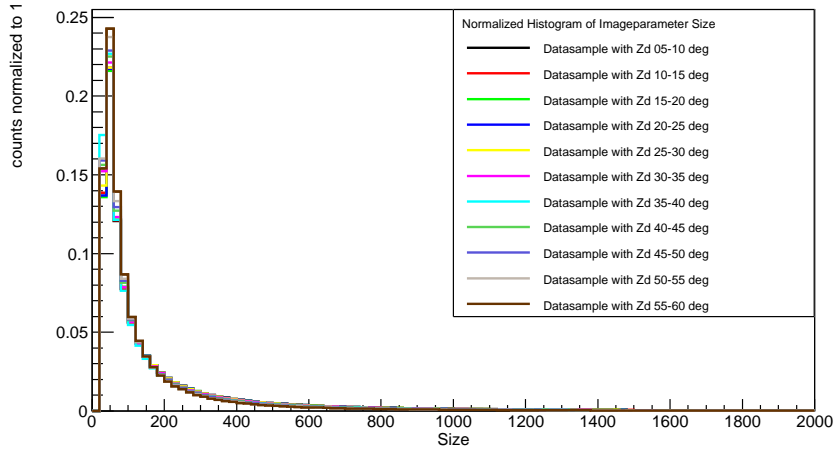
The change of the normalized distribution of the image parameter *Conc_{COG}* is shown in Figure 13(a). One can see that the distribution becomes wider for higher zenith distance. Also the mean value shifts to higher values. This also can be seen in Figure 13(b), where the mean value is fitted with a parabolic fit ($\overline{Conc_{COG}} = \alpha + \beta \cdot (ZD)^2$). This fit is also used to correct the background suppression for high zenith distance. The result of the fit is:

$$\alpha = 0.244802 \pm 0.00248356$$

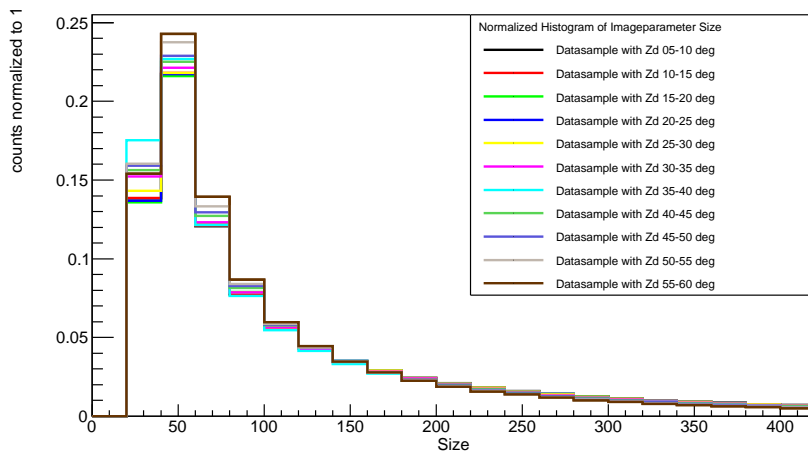
$$\beta = 1.97124 \cdot 10^{-5} \pm 1.48123 \cdot 10^{-6}$$

The zenith dependent background cut for the parameter *Conc_{COG}* is:

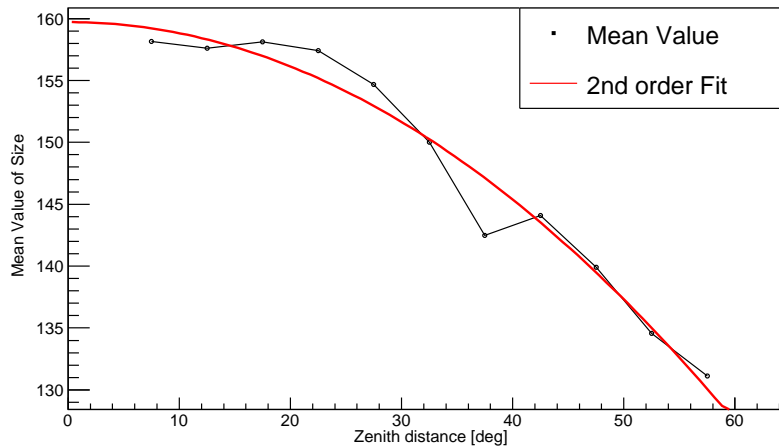
$$Conc_{COG} - 1.97124 \cdot 10^{-5} \cdot (Zd)^2 > 0.15$$



(a)

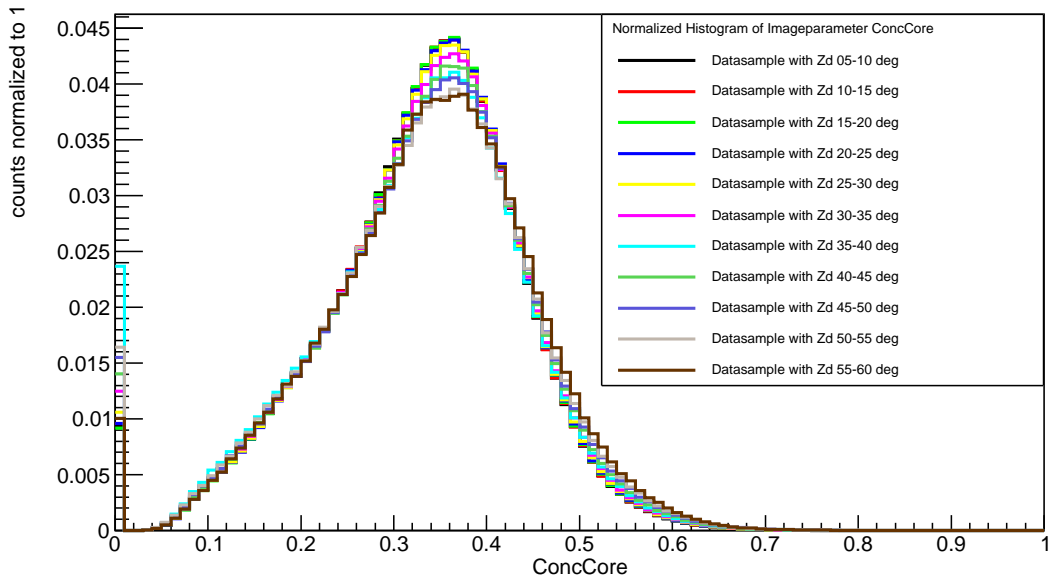


(b)

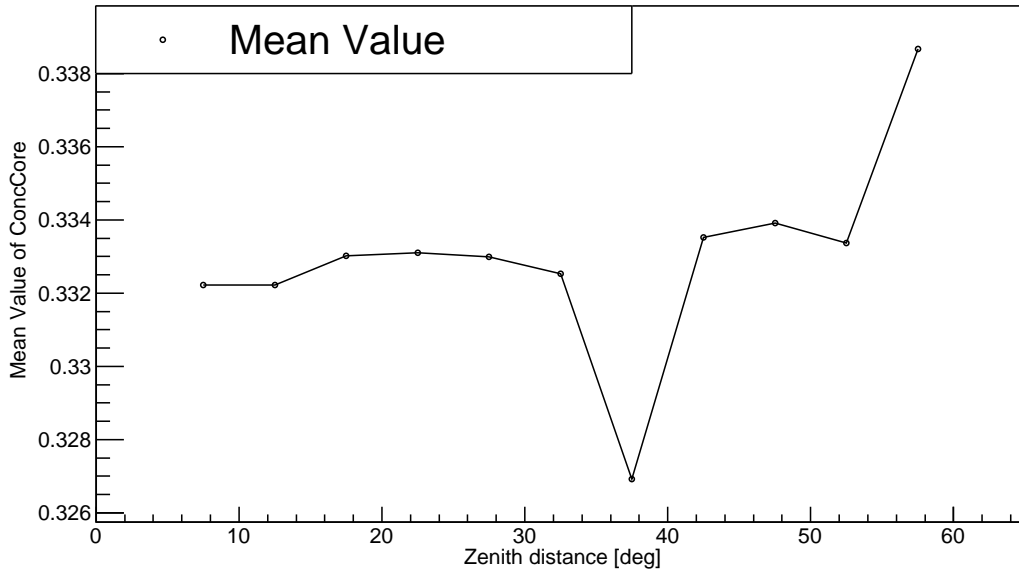


(c)

FIG. 11: Distribution of the image parameter $Size$ normalized to one for the different zenith distance ranges on the upper plot and a zoomed version in the middle plot. The lower plot shows the mean value of the distribution as a function of the zenith distance

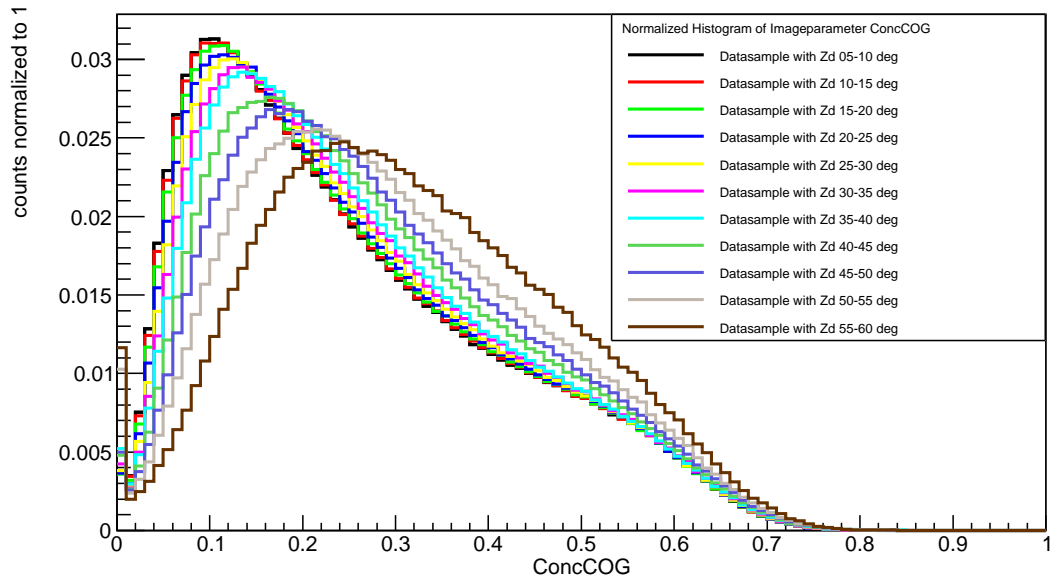


(a)

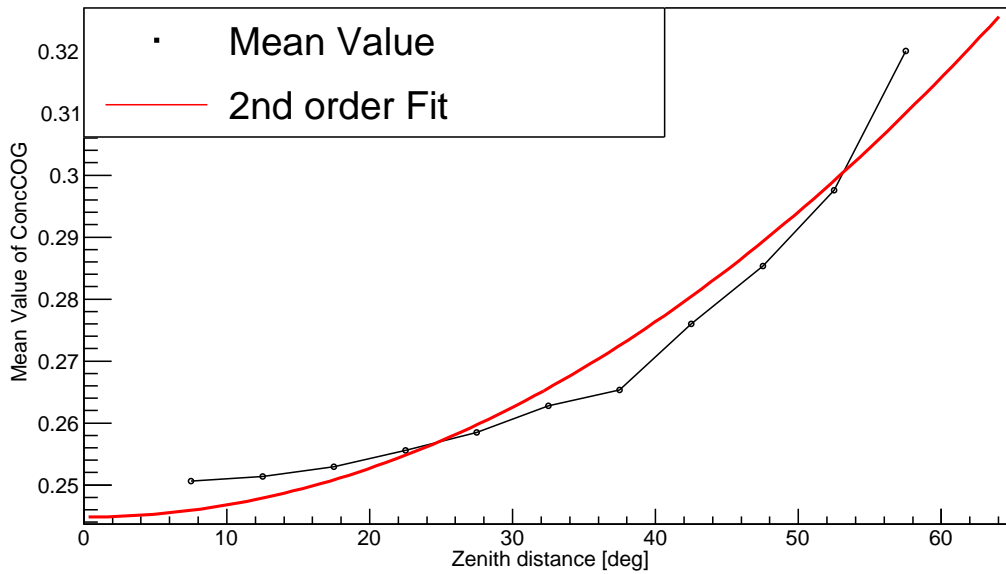


(b)

FIG. 12: The distribution of the image parameter $Conc_{core}$ normalized to one for the different zenith distance ranges is shown on the upper plot. The lower plot shows the mean value of the distribution as a function of the zenith distance



(a)



(b)

FIG. 13: The distribution of the image parameter $ConcCOG$ normalized to one for the different zenith distance ranges is shown on the upper plot. The lower plot shows the mean value of the distribution as a function of the zenith distance.

4 Results

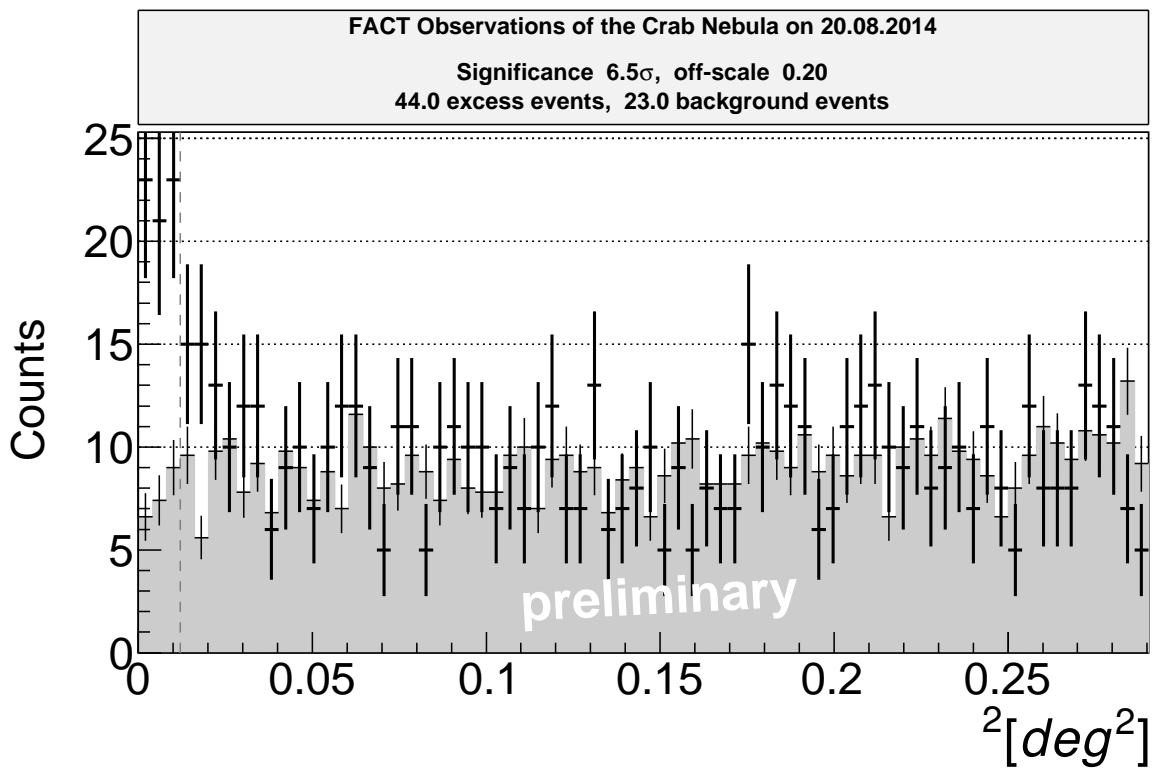
4.1 Crab Nebula

A thetasquaredplot of Crab observations during the night of 20.08.2014 is shown in Figure 14(a) with the normal background suppression and in Figure 14(b) with the zenith distance dependent background cuts. The ontime of this observation was about 1.3 h and the zenith distance was between 42.56 deg and 62.34 deg. One can see that with the new background suppression the number of background events are reduced from 23 to 14.2 but also the excess events are reduced from 44.0 to 36.8. In Figure 15, another thetasquaredplot for both background suppressions is shown. This observation was on the 14.11.2014 and the ontime was 3.7 h. The difference is that this time the zenith distance was between 6.36 deg and 33.99 deg and because of this much lower zenith distance the zenith distance dependent background cuts do not have so much impact as for larger values. In this case, the number of background events drop, from 50.4 to 44.6.

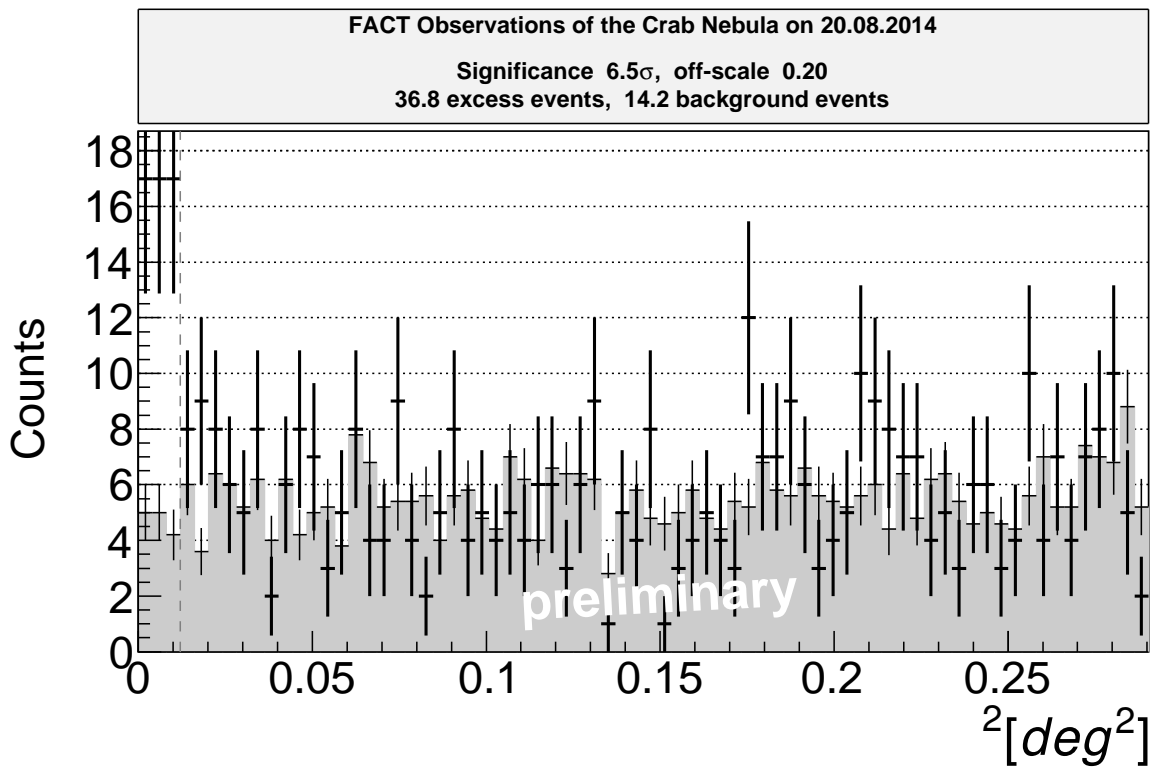
A daily light curve of the Crab observations from 14.12.2012 to 11.03.2016 is shown in Figure 16. The red points of the light curve represent the analysis with the zenith distance dependent background suppression and the blue ones the standard analysis. One can see that the value of the excess rate and the error bars getting smaller for the new background suppression. Also one can see the impact of the analysis change in May 2014. The mean value of the excess rate of the Crab, called Crabunit, is higher for new analysis. Figure 17 shows a histogram of the excess rates (upper plot) and a histogram of the excess rate errors (lower plot) of the Crab light curve after the analysis change. This plot also shows that the error of the excess rate decreases by using zenith dependent background suppression.

4.2 1ES 1959+650

1ES 1959+650 is a BL Lac object with a redshift of $z=0.048$ and was first detected as a TeV gamma-ray source with the Utah Seven Telescope Array detector during observations from May 1998 until August 1998. [22] 1ES 1959+650 is a highly variable source that culminates for La Palma at about 35 deg. The upper plot in Figure 18 shows the light curve from the years 2013, 2014, 2015 and 2016. For the old background suppression the blue points are used and the red ones show the excess rate with the zenith distance dependent background suppression. The first two years are shown in yearly binning, while 2015 and 2016 are shown in daily binning. There are only nights included in the graph with an ontime above 1 hour. Like it has been seen on the Crab Nebula light curve, also for the light curve of 1ES 1959+650 the zenith distance dependent background suppression reduces the error bars of the light curve and does not change the shape of the light curve. One can see that 1ES 1959+650 was in an inactive state in the first two years of FACT observations. In 2015 this changed and the gamma events of 1ES 1959+650 began to get significantly visible for the FACT telescope. The year 2015 is enhanced shown on the middle of Figure 18. The excess rate rises in some days to a value above $12 \frac{\text{events}}{\text{h}}$ with the zenith distance dependent background suppression. The measurements of 2016 show that 1ES 1959+650 was still active a high variable source. There are two nights were the excess rate rises above a value of $50 \frac{\text{events}}{\text{h}}$. This flaring nights were the 12. June and 11. July 2016. The thetasquaredplot of the second flaring night is shown in figure 19, for the normal and the zenith distance dependent background suppression. Through the new background suppression cuts the number of background events dropped form 43.2 to 29 events and the excess events from 226.8 to 195.

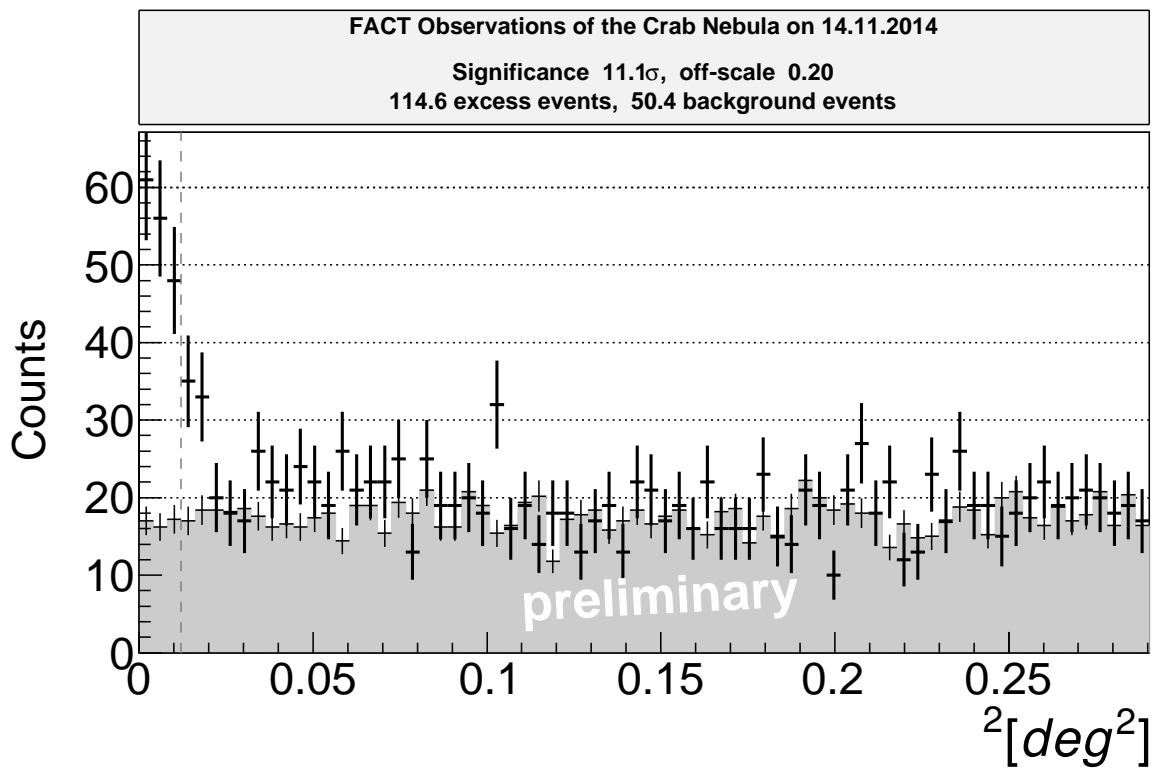


(a) normal background suppression

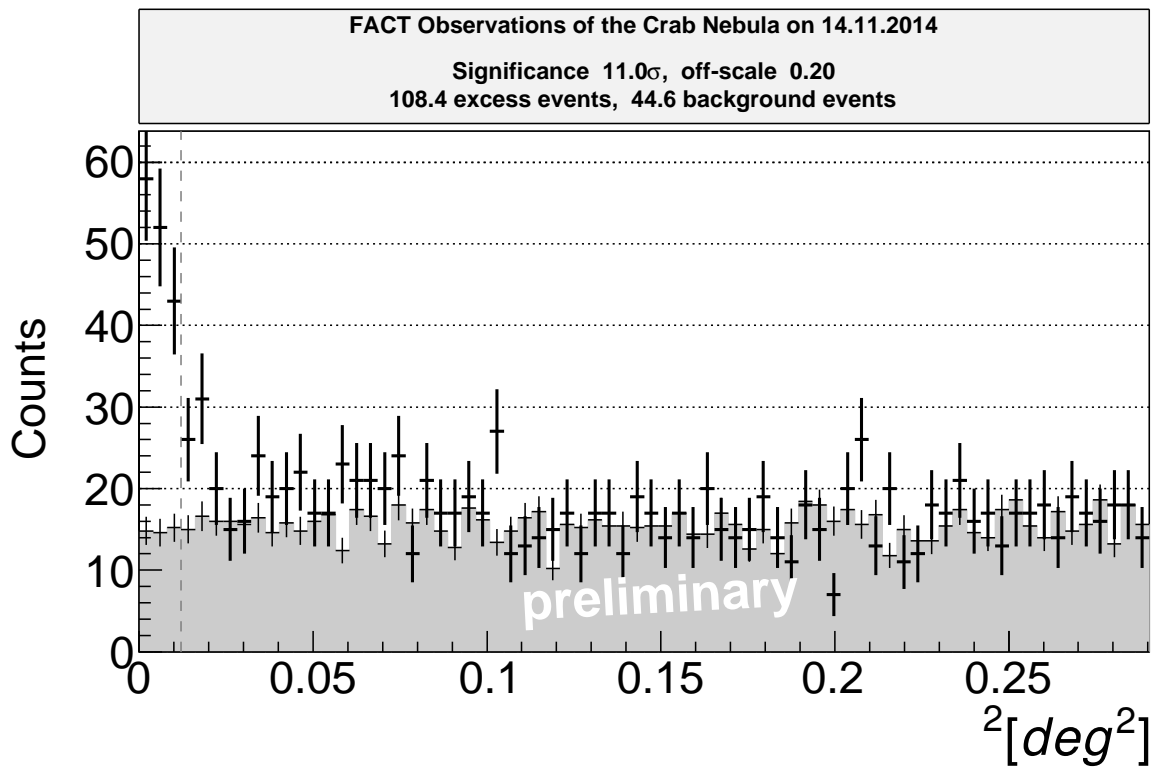


(b) zenith distance dependent background suppression

FIG. 14: Thetasquareplot of Crab observations on 20.08.2014 with an ontime of 1.3 h and a zenith distance range between 42 deg and 64 deg. The upper plot uses the normal background suppression and the lower plot the zenith distance dependent background suppression.



(a) normal background suppression



(b) zenith distance dependent background suppression

FIG. 15: Thetasquareplot of Crab observations on 14.11.2014 with an ontime of 3.7 h and a zenith distance range between 6 deg and 34 deg. The upper plot uses the normal background suppression and the lower plot the zenith distance dependent background suppression.

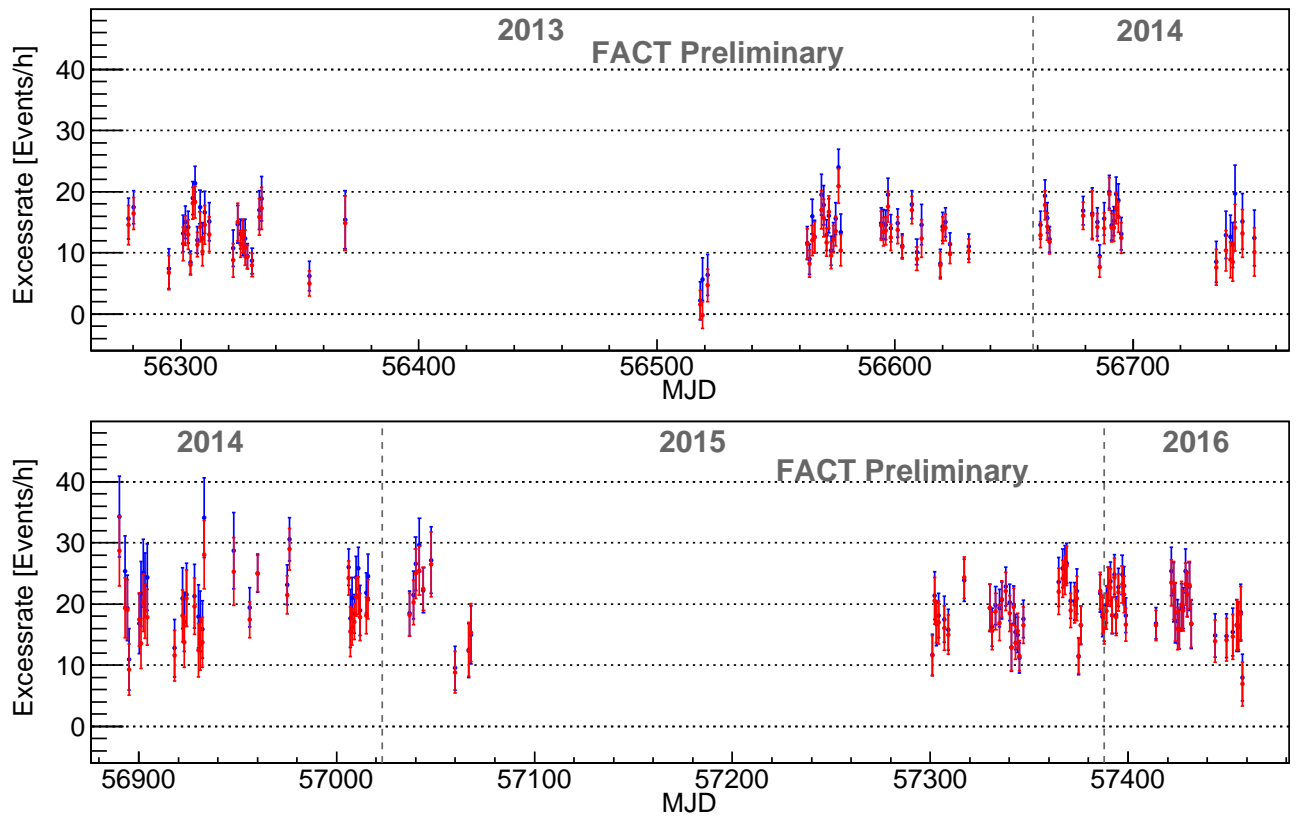


FIG. 16: Daily light curve of observations of the Crab Nebula from 14.12.2012 to 11.03.2016. The red points are the excess rate for a zenith distance dependent background cut. The blue points are made with the old background suppression. The upper plot shows data before the analysis were changed, the lower plot the time after this change.

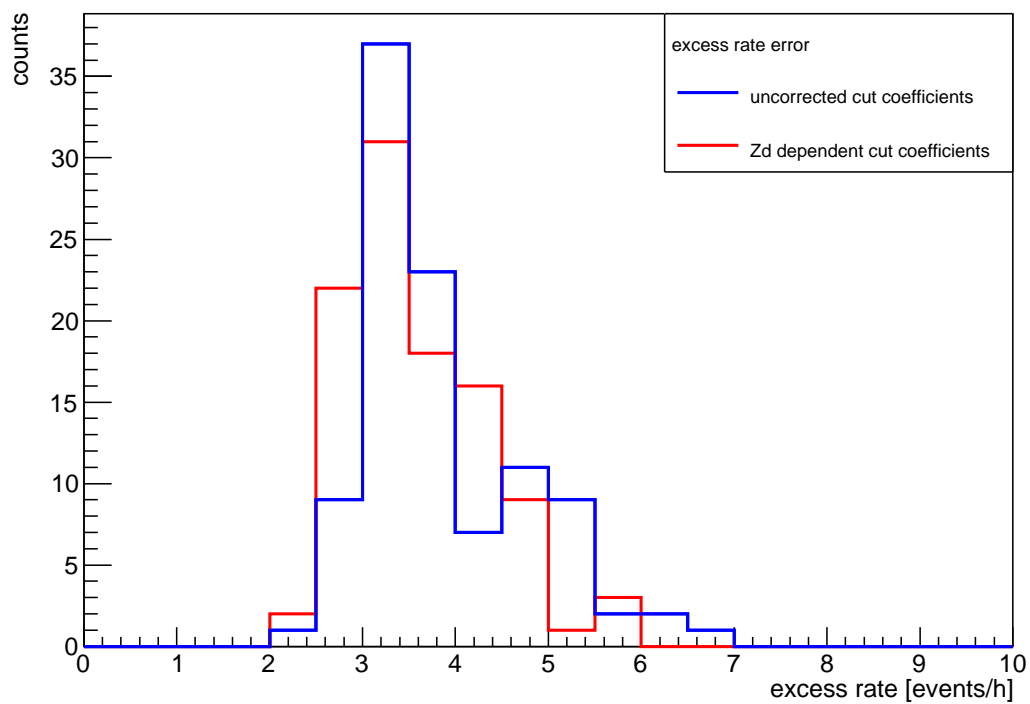
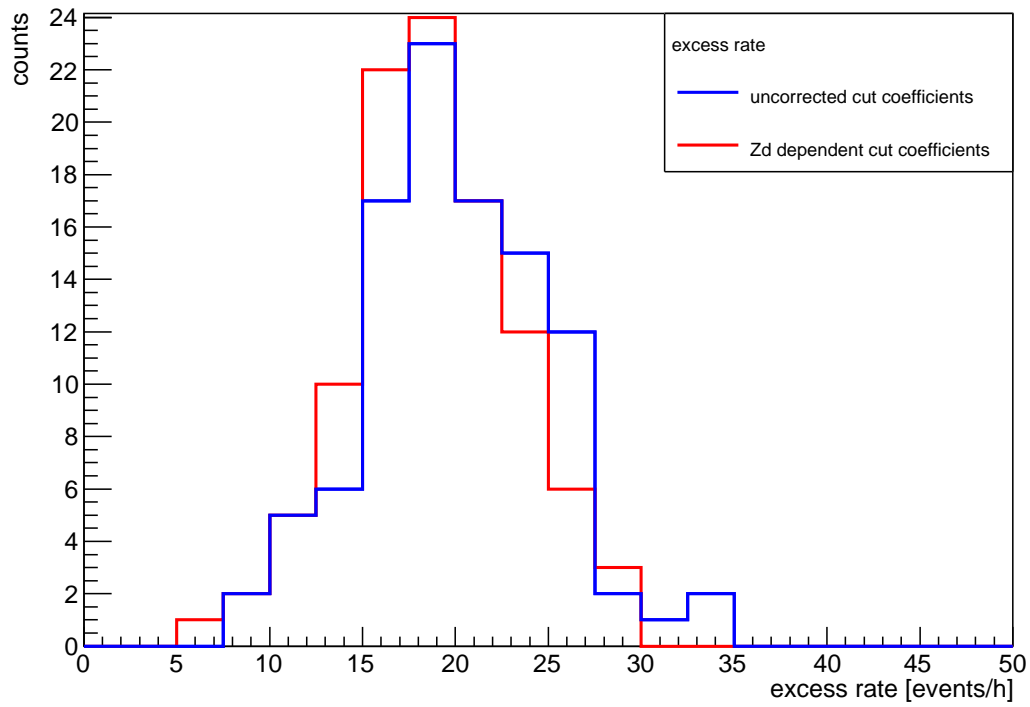


FIG. 17: Histogram of the excess rate (upper plot) and the excess rate error (lower plot) of the Crab Nebula light curve for observations after March 2014.

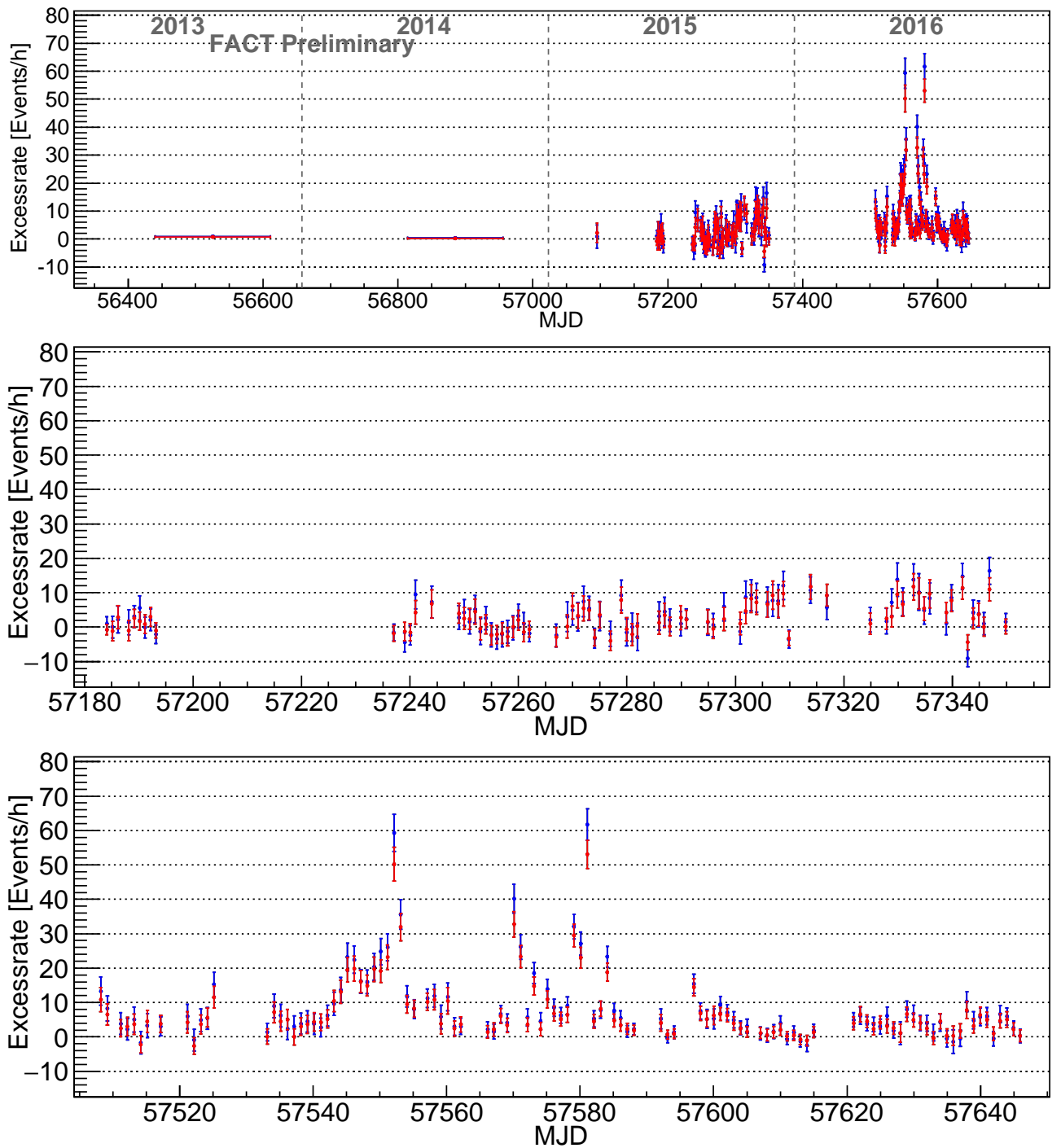
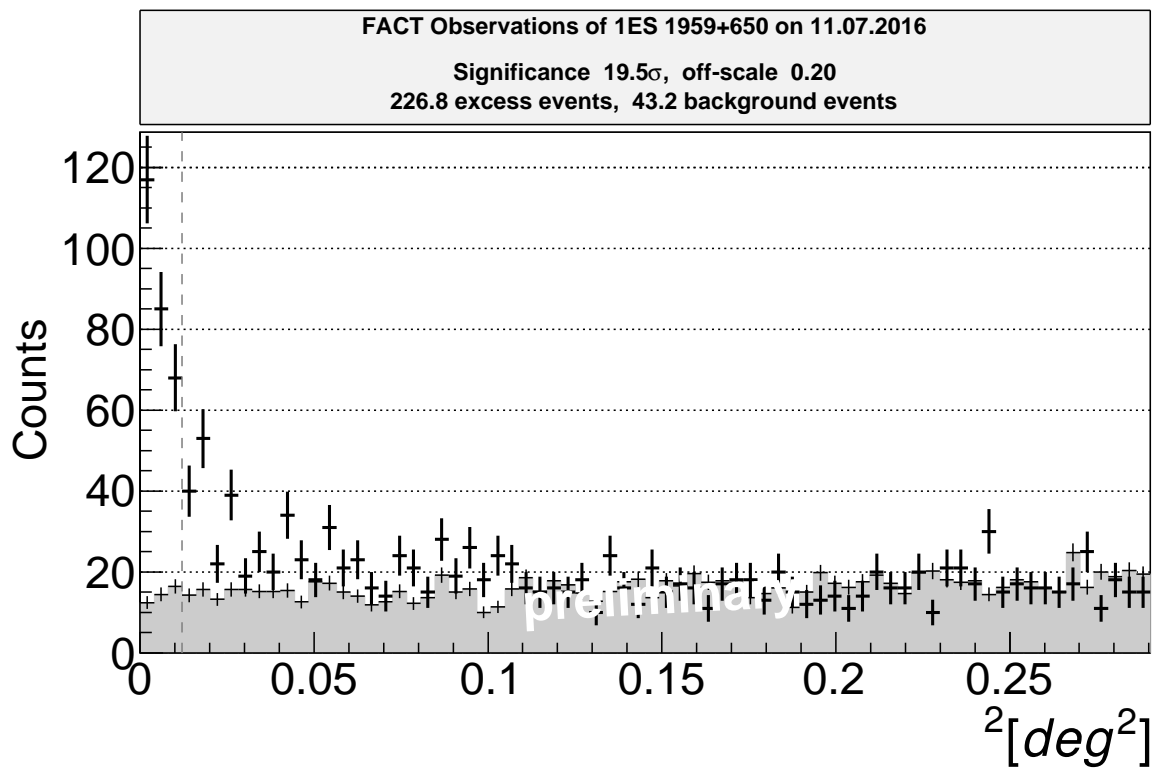
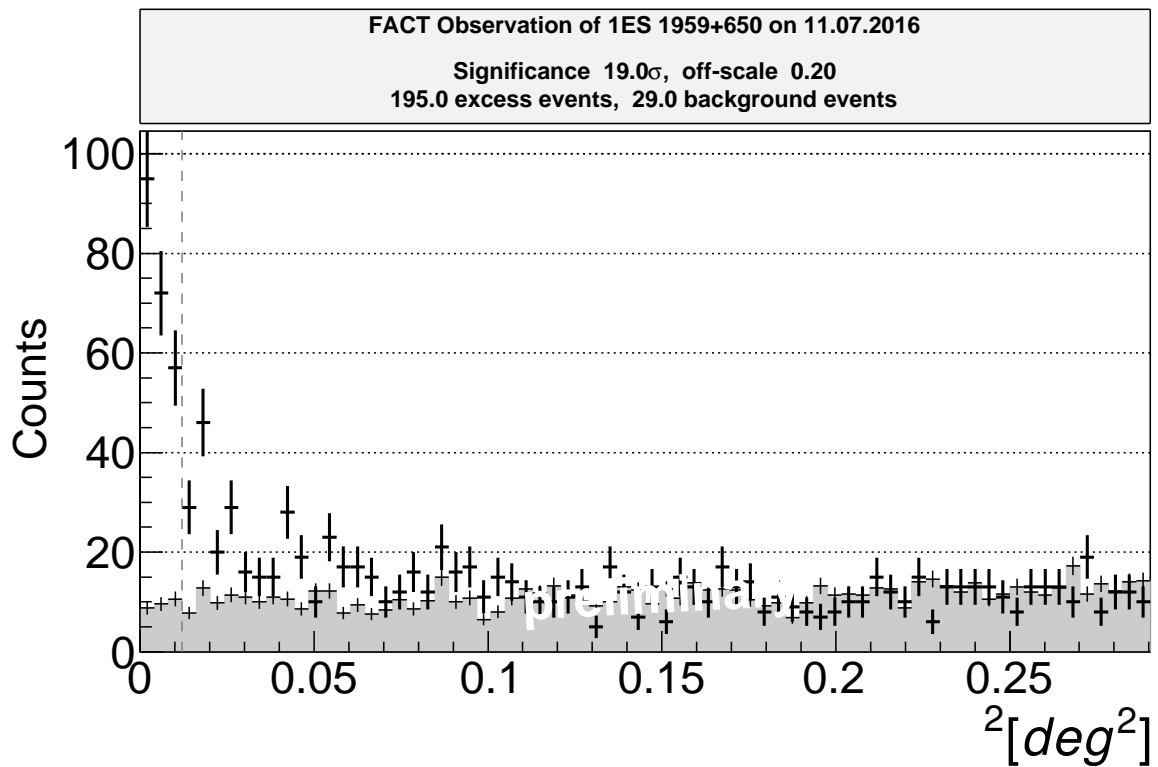


FIG. 18: Light curve of observations of the source 1ES 1959+650 from 27.05.2013 to 18.09.2016. The red points are the excess rate for a zenith distance dependent background cut. The blue points are made with the old background suppression. Observations of the year 2013 and 2014 are summarized yearly, because 1ES 1959+650 did not show any activity during this time. All data points of 2015 and 2016 are in daily binning. The 2 active years of 1ES 1959+650 are again plotted in the middle (2015) and the lower (2016) plot.



(a) normal background suppression



(b) zenith distance dependent background suppression

FIG. 19: Histogram of θ^2 for the flaring night of 1ES 1959+650 on 11.07.2016 with an ontime of 3.7 h. The upper plot uses the normal background suppression and the lower plot the zenith distance dependent background suppression.

5 Summary and Outlook

Blazars like 1ES1959+650 have been monitored by FACT at TeV energies. Culminating at 35 degree in La Palma, this source challenges the analysis. Background cuts for large zenith distance are needed.

5.1 Zenith Dependent Cuts

To investigate the zenith distance dependence of the background suppression, a dataset of the Crab Nebula data was investigated. For this, the distributions of the image parameters used in the background suppression were analysed. Studying the mean values of these distributions, zenith distance dependent correction parameters were added to the original cuts of the background suppression. The image parameters that show a zenith dependency are *Area*, *Size* and *Conc_{COG}*. The zenith distance dependent background suppression cuts are:

$$\begin{aligned} 0.18 < SlopeSpreadWeighted < 0.68 \\ \log_{10}(Area + 4.6658 \cdot 10^{-2} \cdot (ZD)^2) < (\log_{10}(Size + 1.54657 \cdot 10^{-2} \cdot (ZD)^2) - 2) \cdot 1.1 - 1.55 \\ Conc_{core} > 0.13 \\ Conc_{COG} - 1.97124 \cdot 10^{-5} \cdot (Zd)^2 > 0.15 \end{aligned}$$

Light curves from 2013 till 2016 were studied for the data of the Crab Nebula and 1ES 1959+650. They show that the error bars of the daily excess rates decrease by using the zenith distance dependent background suppression and the shape of the light curve does not change. The used method to determine an zenith dependency is a simple way to improve the analysis of large zenith distance data. As the mean value of a distribution is not ideal to describe a distribution, the zenith depended background cut coefficients should be fitted in a next step to optimize the cuts for signal events by simultaneously reducing the background events.

In a next step Monte Carlo events should be simulated for each monitored source for a large zenith distance range. With the help of them the new background suppression cuts could be cross-checked with simulated data or the background suppression cuts could be adapted by using a dataset of Monte Carlo Simulations. These simulation are also needed to reconstruct the energy of the events and calculate the flux. Correlating the TeV fluxes with other wavelengths, current theories of the underlying processes in the relativistic jets of AGN can be constrained.

5.2 Flaring Activity of 1ES 1959+650

An excellent data sample for such studies is available from a recent flaring activity of the blazar 1ES 1959+650. Figure 20 shows the excess rates of the long time behaviour (upper plot) and the flaring activities. In 2016, FACT sent five Astronomer's Telegrams¹ (ATEL) to the community because of increasing excess rates of 1ES 1959+650. The sent ATELs are marked in the daily light curve (lower plot). The dashed blue line shows the excess rate of the major outburst in May 2002. The HEGRA stereoscopic system [1] and the Whipple 10 m telescope [14] observed at this time a highly variable and strong flare of this source. One can see that the two highest flaring nights of 2016 have even higher excess rates and by sending ATELs, there is a big chance

¹short-notice publication system for professional astronomy <http://www.astronomersteam.org/> [23]

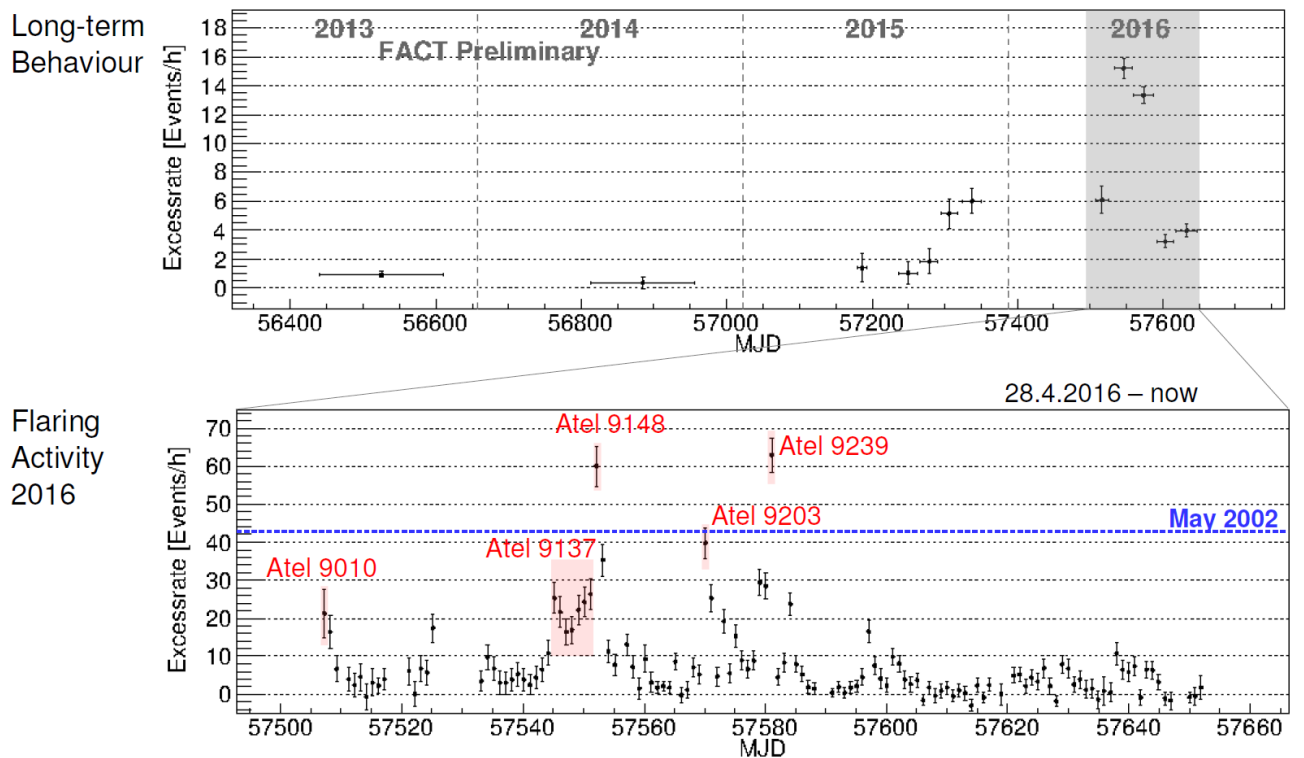


FIG. 20: Light curve of 1ES 1959+65. The upper plot shows the long time behaviour of the source. In the lower plot the daily light curve of 2016 is shown. The nights where FACT was sending an ATEL are highlighted. Also the excess rate of the famous flaring night of May 2002 is shown as the blue dashed line. The plot is taken from [10].

to have simultaneously data in several energy ranges. This gives the opportunity to combine these data for multi-wavelength studies. The 2002 flare was investigated in a multi-wavelength campaign. The data of Whipple and HEGRA in the TeV range, X-ray data of the X-ray telescope Rossi X-Ray Timing Explorer, optical data of the Boltwood and Abastumani observatories and radio data of the Michigan Radio Astronomy Observatory were combined there. In general, the X-rays and gamma rays showed a correlation, but an orphan gamma-ray flare was found. A Correlation of the optical data with the X-ray and gamma ray was not found, and the radio data were constant within their errors. An orphan flare is not compatible with the most simple one-zone SSC models.[15]

While SSC models expect a correlation between the low and high energy peak, hadronic models can explain more complex correlations. Those models on the other hand predict the occurrence of neutrinos. Therefore multi-messenger studies are also very interesting in that context. The AMANDA neutrino telescope detected high-energy neutrinos during the flare of 2002, but the statistical significant of this observation is not reliable. By combining TeV data with neutrino data one can find indications of the underlying processes in the relativistic jets. The proton models expect pion decays in the jet, which would cause the production of neutrinos. [13]

Currently, the FACT data of the 1ES 1959+650 flaring activity are analysed in studies which combine these data with IceCube, Swift, Fermi and optical telescope observations.

Bibliography

- [1] F. Aharonian, A. Akhperjanian, M. Beilicke, K. Bernlöhr, H.-G. Börst, H. Bojahr, O. Bolz, T. Coarasa, J. L. Contreras, J. Cortina, S. Denninghoff, M. V. Fonseca, M. Girma, N. Göting, G. Heinzlmann, G. Hermann, A. Heusler, W. Hofmann, D. Horns, I. Jung, R. Kanakyan, M. Kestel, A. Kohnle, A. Konopelko, H. Kornmeyer, D. Kranich, H. Lampeitl, M. Lopez, E. Lorenz, F. Lucarelli, O. Mang, H. Meyer, R. Mirzoyan, A. Moralejo, E. Ona-Wilhelmi, M. Panter, A. Plyasheshnikov, G. Pühlhofer, R. de los Reyes, W. Rhode, J. Ripken, J. Robrade, G. Rowell, V. Sahakian, M. Samorski, M. Schilling, M. Siems, D. Sobzynska, W. Stamm, M. Tluczykont, V. Vitale, H. J. Völk, C. A. Wiedner, and W. Wittek. Detection of TeV gamma-rays from the BL lac 1es 1959+650 in its low states and during a major outburst in 2002. *Astronomy & Astrophysics*, 406(1):L9–L13, jul 2003.
- [2] A. M. Atoyan and F. A. Aharonian. On the mechanisms of gamma radiation in the crab nebula. *Monthly Notices of the Royal Astronomical Society*, 278(2):525–541, jan 1996.
- [3] V. Beckmann and C. Shrader. *Active Galactic Nuclei*. Wiley, 2013.
- [4] A Biland, T Bretz, J Buß, V Commichau, L Djambazov, D Dorner, S Einecke, D Eisenacher, J Freiwald, O Grimm, H von Gunten, C Haller, C Hempfling, D Hildebrand, G Hughes, U Horisberger, M L Knoetig, T Krähenbühl, W Luster mann, E Lyard, K Mannheim, K Meier, S Mueller, D Neise, A K Overkemping, A Paravac, F Pauss, W Rhode, U Röser, J P Stucki, T Steinbring, F Temme, J Thaele, P Vogler, R Walter, and Q Weitzel. Calibration and performance of the photon sensor response of fact — the first g-apd cherenkov telescope. *Journal of Instrumentation*, 9(10):P10012, 2014.
- [5] Heidrun Bojahr. *Suche nach TeV-Blazaren mit dem HEGRA-System der abbildenden Cherenkov-Teleskope*. dissertation, Bergische Universität Wuppertal, 2002.
- [6] T. Bretz and D. Dorner and. MARS - CheObs ed. — a flexible software framework for future cherenkov telescopes. In *Astroparticle, Particle and Space Physics, Detectors and Medical Physics Applications*. World Scientific Pub Co Pte Lt, apr 2010.
- [7] T. Bretz J. Buss S. Einecke D. Eisenacher D. Hildebrand M. L. Knötig T. Krähenbühl W. Luster mann K. Mannheim K. Meier D. Neise A.-K. Overkemping A. Paravac F. Pauss W. Rhode M. Ribordy T. Steinbring F. Temme J. Thaele R. Walter Q. Weitzel M. Zänglein D. Dorner, A. Biland. Fact - long-term monitoring of bright tev-blazars. *ICRC*, 2013.
- [8] D. Dorner, M. L. Ahnen, M. Bergmann, A. Biland, M. Balbo, T. Bretz, J. Buss, S. Einecke, J. Freiwald, C. Hempfling, D. Hildebrand, G. Hughes, W. Luster mann, K. Mannheim, K. Meier, S. Mueller, D. Neise, A. Neronov, A. K. Overkemping, A. Paravac, F. Pauss, W. Rhode, T. Steinbring, F. Temme, J. Thaele, S. Toscano, P. Vogler, R. Walter, and A. Wilbert. Fact - monitoring blazars at very high energies, 2015.
- [9] B. L. Fanaroff and J. M. Riley. The morphology of extragalactic radio sources of high and low luminosity. *Monthly Notices of the Royal Astronomical Society*, 167:31P–36P, May 1974.
- [10] D. Dorner for the FACT Collaboration. Triggering integral observations with the fact monitoring program. *Integral 2016 Conference*, 2016.

- [11] M.-L. Knoetig for the FACT Collaboration. Fact - long-term stability and observations during strong moon light. *ICRC*, 2013.
- [12] Christian Fruck and Markus Gaug. Atmospheric monitoring in MAGIC and data corrections. *EPJ Web of Conferences*, 89:02003, 2015.
- [13] Francis Halzen and Dan Hooper. High energy neutrinos from the TeV blazar 1es 1959+650. *Astroparticle Physics*, 23(6):537–542, jul 2005.
- [14] J. Holder, I. H. Bond, P. J. Boyle, S. M. Bradbury, J. H. Buckley, D. A. Carter-Lewis, W. Cui, C. Dowdall, C. Duke, I. de la Calle Perez, A. Falcone, D. J. Fegan, S. J. Fegan, J. P. Finley, L. Fortson, J. A. Gaidos, K. Gibbs, S. Gammell, J. Hall, T. A. Hall, A. M. Hillas, D. Horan, M. Jordan, M. Kertzman, D. Kieda, J. Kildea, J. Knapp, K. Kosack, H. Krawczynski, F. Krennrich, S. LeBohec, E. T. Linton, J. Lloyd-Evans, P. Moriarty, D. Müller, T. N. Nagai, R. Ong, M. Page, R. Pallassini, D. Petry, B. Power-Mooney, J. Quinn, P. Rebillot, P. T. Reynolds, H. J. Rose, M. Schroedter, G. H. Sembroski, S. P. Swordy, V. V. Vassiliev, S. P. Wakely, G. Walker, and T. C. Weekes. Detection of TeV gamma rays from the BL lacertae object 1ES 1959+650 with the Whipple 10 meter telescope. *The Astrophysical Journal*, 583(1):L9–L12, jan 2003.
- [15] H. Krawczynski, S. B. Hughes, D. Horan, F. Aharonian, M. F. Aller, H. Aller, P. Boltwood, J. Buckley, P. Coppi, G. Fossati, N. Gotting, J. Holder, D. Horns, O. M. Kurtanidze, A. P. Marscher, M. Nikolashvili, R. A. Remillard, A. Sadun, and M. Schroder. Multiwavelength observations of strong flares from the TeV blazar 1es 1959+650. *The Astrophysical Journal*, 601(1):151–164, jan 2004.
- [16] A. Lawrence. Classification of active galaxies and the prospect of a unified phenomenology. *Publications of the Astronomical Society of the Pacific*, 99:309–334, May 1987.
- [17] R.W. Lessard, J.H. Buckley, V. Connaughton, and S. Le Bohec. A new analysis method for reconstructing the arrival direction of TeV gamma rays using a single imaging atmospheric cherenkov telescope. *Astroparticle Physics*, 15(1):1–18, mar 2001.
- [18] K. Mannheim. Possible production of high-energy gamma rays from proton acceleration in the extragalactic radio source markarian 501. *Science*, 279(5351):684–686, jan 1998.
- [19] N. U. Mayall. The crab nebula, a probable supernova. *Leaflet of the Astronomical Society of the Pacific*, 3:145, 1939.
- [20] Katja Meier, A. Biland, T. Bretz, J. Buss, D. Dorner, S. Einecke, D. Eisenacher, D. Hildebrand, M. L. Knoetig, T. Krähenbühl, W. Lusterhann, K. Mannheim, D. Neise, A.-K. Overkemping, A. Paravac, F. Pauss, W. Rhode, M. Ribordy, T. Steinbring, F. Temme, J. Thaele, P. Vogler, R. Walter, Q. Weitzel, and M. Zänglein. FACT — LONGTERM MONITORING OF BRIGHT TeV BLAZARS. *Acta Polytechnica*, 54(3):210–213, jun 2014.
- [21] Javier Lopez Munoz. *Measurement of the invariance of the speed of light observing the active galactic nucleus Mkn421 with the MAGIC Telescope*. dissertation, Universitat Autònoma de Barcelona, 2006.
- [22] T. Nishiyama. Detection of a new TeV gamma-ray source of BL Lac object 1ES 1959+650. *International Cosmic Ray Conference*, 3:370, August 1999.

- [23] Robert E. Rutledge. The astronomer's telegram: A web-based short-notice publication system for the professional astronomical community. *Publications of the Astronomical Society of the Pacific*, 110(748):754–756, jun 1998.
- [24] Marek Sikora. Blazars. In *AIP Conference Proceedings*. AIP Publishing, 2001.
- [25] D. A. Turnshek. Properties of the broad absorption-line QSOs. *The Astrophysical Journal*, 280:51–65, May 1984.
- [26] C. M. Urry and P. Padovani. Unified Schemes for Radio-Loud Active Galactic Nuclei. *Publications of the Astronomical Society of the Pacific*, 107:803, September 1995.
- [27] T. C. Weekes, M. F. Cawley, D. J. Fegan, K. G. Gibbs, A. M. Hillas, P. W. Kowk, R. C. Lamb, D. A. Lewis, D. Macomb, N. A. Porter, P. T. Reynolds, and G. Vacanti. Observation of TeV gamma rays from the crab nebula using the atmospheric cerenkov imaging technique. *The Astrophysical Journal*, 342:379, jul 1989.
- [28] T.C. Weekes. *Very High Energy Gamma-Ray Astronomy*. Series in Astronomy and Astrophysics. CRC Press, 2003.

6 Acknowledgement

First of all, I would like to thank Prof. Dr. Karl Mannheim for giving me the opportunity to write this thesis in the field of astronomy under his supervision.

I want to express a special gratitude to Dr. Daniela Dorner for guiding me through this thesis, for helping with all questions which have arisen and for a lot of useful discussions. Without her guidance and persistent help this thesis would not have been possible.

I also would like to thank Dr. Dorit Glawion for introducing me in the use of Root and for all the helpful hints.

Furthermore, I would like to thank the entire FACT collaboration for the warm welcoming of new members, the fruitful discussions and for providing the data.

Additionally, I want to thank Tobias Herbst for the helpful discussion and the support in case of problems.

Many thanks go to all colleagues of the chair of astronomy for the nice working atmosphere, useful discussions and their help.

Finally, I want to thank my family and friends for their great confidence and support.

Selbstständigkeitserklärung

Ich versichere, die vorliegende Arbeit selbstständig und nach allgemeiner Studien- und Prüfungsordnung für die Bachelor- und Masterstudiengänge (ASPO) an der Julius-Maximilians-Universität Würzburg verfasst und keine anderen als die angegebenen Quellen und Hilfsmittel benutzt, sowie keiner anderen Prüfungsbehörde zur Erlangung eines akademischen Grades vorgelegt zu haben.

Bernd Schleicher, Würzburg, den 31.03.2017